



THE UNIVERSITY *of* EDINBURGH

Edinburgh Research Explorer

Subsidence and exhumation of the Mesozoic Qiangtang Basin: Implications for the growth of the Tibetan plateau

Citation for published version:

Zhang, J, Sinclair, H, Li, Y, Wang, C, Persano, C, Qian, X, Han, Z, Yao, X & Duan, Y 2019, 'Subsidence and exhumation of the Mesozoic Qiangtang Basin: Implications for the growth of the Tibetan plateau', *Basin Research*, vol. 31, no. 4, pp. 754-781. <https://doi.org/10.1111/bre.12343>

Digital Object Identifier (DOI):

[10.1111/bre.12343](https://doi.org/10.1111/bre.12343)

Link:

[Link to publication record in Edinburgh Research Explorer](#)

Document Version:

Peer reviewed version

Published In:

Basin Research

General rights

Copyright for the publications made accessible via the Edinburgh Research Explorer is retained by the author(s) and / or other copyright owners and it is a condition of accessing these publications that users recognise and abide by the legal requirements associated with these rights.

Take down policy

The University of Edinburgh has made every reasonable effort to ensure that Edinburgh Research Explorer content complies with UK legislation. If you believe that the public display of this file breaches copyright please contact openaccess@ed.ac.uk providing details, and we will remove access to the work immediately and investigate your claim.





Subsidence and exhumation of the Mesozoic Qiangtang Basin: Implications for the growth of the Tibetan plateau

Journal:	<i>Basin Research</i>
Manuscript ID	BRE-020-2018.R3
Manuscript Type:	Original Article
Date Submitted by the Author:	n/a
Complete List of Authors:	<p>Zhang, Jiawei; China University of Geosciences Beijing, State Key Laboratory of Biogeology and Environmental Geology; Institute of Geology, China Earthquake Administration, State Key Laboratory of Earthquake Dynamics</p> <p>Sinclair, Hugh; The University of Edinburgh, Grant Institute, School of GeoSciences</p> <p>Li, Yalin; China University of Geosciences Beijing, State Key Laboratory of Biogeology and Environmental Geology</p> <p>Wang, Chengshan; China University of Geosciences Beijing, State Key Laboratory of Biogeology and Environmental Geology</p> <p>Persano, Cristina; University of Glasgow College of Science and Engineering</p> <p>Qian, Xinyu; China University of Geosciences Beijing, State Key Laboratory of Biogeology and Environmental Geology</p> <p>Han, Zhongpeng; China University of Geosciences Beijing, State Key Laboratory of Biogeology and Environmental Geology</p> <p>Yao, Xiang; China University of Geosciences Beijing, State Key Laboratory of Geological Processes and Mineral Resources</p> <p>Duan, Yaoyao; Chengdu Centre of Geology and Mineral Resources</p>
Keywords:	Qiangtang, Subsidence, Apatite fission track, Crustal thickening

SCHOLARONE™
Manuscripts

Jiawei Zhang^{a, b} Hugh D. Sinclair^c Yalin Li^{a, *} Chengshan Wang^a Cristina
 Persano^d Xinyu Qian^a Zhongpeng Han^a Xiang Yao^e Yaoyao Duan^f

E-mail address: liyalin@cugb.edu.cn (Yalin Li)

ABSTRACT

The subsidence and exhumation histories of the Qiangtang Basin and their contributions to the early evolution of the Tibetan plateau are vigorously debated. This paper reconstructs the subsidence history of the Mesozoic Qiangtang Basin with eleven selected composite stratigraphic sections and constrains the first stage of cooling using apatite fission track data. Facies analysis, biostratigraphy, paleo-environment interpretation, and paleo-water depth estimation are **integrated to create** eleven composite sections **through** the basin. **Backstripped** subsidence **calculations** combined with previous work on sediment provenance and timing of deformation, show that the evolution of the Mesozoic Qiangtang Basin can be divided into two stages. From Late Triassic to Early Jurassic times, the North Qiangtang was a retro-foreland basin. In contrast, the South Qiangtang was a collisional **pro-foreland** basin. During Middle Jurassic to Early Cretaceous times, **the North Qiangtang is interpreted as a hinterland basin between the Jinsha orogen and the Central Uplift; the South Qiangtang was controlled by subduction of Meso-Tethyan Ocean lithosphere and associated dynamic topography combined with loading from the Central Uplift.** Detrital apatite fission track ages **from Mesozoic sandstones** concentrate in late Early to Late Cretaceous (120.9-84.1 Ma) and Paleogene-Eocene (65.4-40.1 Ma). Thermal history modelling results record Early Cretaceous rapid cooling; the termination of subsidence and onset of exhumation of the Mesozoic Qiangtang Basin suggest that the accumulation of crustal thickening in central Tibet probably initiated during Late Jurassic-Early **Cretaceous times** (150-130 Ma), involving underthrusting of both the

1
2
3
4
5
6
7
8
9
10
11
12
13
14
15
16
17
18
19
20
21
22
23
24
25
26
27
28
29
30
31
32
33
34
35
36
37
38
39
40
41
42
43
44
45
46
47
48
49
50
51
52
53
54
55
56
57
58
59
60

45 Lhasa and Songpan-Ganze terranes beneath the Qiangtang terrane, or the collision of
46 Amdo terrane.

47 **Keywords:** Qiangtang, Subsidence, Apatite fission track, Crustal thickening

48 **INTRODUCTION**

49 The collision of India with Asia is the most important driving force for the
50 growth of the Tibetan plateau (Argand, 1922; Dewey *et al.*, 1988; Yin & Harrison,
51 2000), with the onset of collision at about 55±10 Ma promoting significant changes in
52 Tibetan plateau height and relief (Currie *et al.*, 2005; Rowley & Currie, 2006; Ding *et*
53 *al.*, 2014, 2017; Wang *et al.*, 2014; Leary *et al.*, 2017). Evidence shows that
54 deformation in the hinterland of the plateau occurred before collision (Murphy *et al.*,
55 1997; Kapp *et al.*, 2005). However, uncertainty remains as to whether this early
56 shortening resulted in moderate or high elevations within the Tibetan plateau prior to
57 the India-Asia collision (Zhang *et al.*, 2012 and references therein). It is reasonable to
58 speculate that the crustal thickening in the central region of the Tibetan plateau had
59 started before Cenozoic times (Zhao *et al.*, 2017). The Qiangtang Basin developed on
60 the overriding plate between two major suture zones (the Bangong Lake-Nujiang
61 suture zone, BNSZ, to the south and the Jinsha River suture zone, JRSZ, to the north,
62 respectively), and is considered to record the early growth of the central Tibetan
63 plateau (Song, 2012; Ren *et al.*, 2015; Zhao *et al.*, 2017). However, Early Mesozoic
64 subsidence and pre-Cenozoic exhumation histories of the Mesozoic marine Qiangtang
65 Basin are unclear, which hinders understanding of the early history of crustal
66 thickening in central Tibet. This is due in large part, to the extremely remote locations

and the strong Cenozoic structural deformation of the stratigraphic successions (Kapp *et al.*, 2003, 2005). Therefore, understanding of the Mesozoic history of the Qiangtang Basin is **variable**. The proposed mechanisms for basin subsidence are dominated by two competing models. **It is proposed that either** the basin formed in an extensional setting on the southern margin of Eurasia during Late Triassic to Early Cretaceous times (e.g., Wang *et al.*, 2004a; Song, 2012), **or that it represents** a foreland basin (e.g. Wang *et al.*, 2001; Li *et al.*, 2002). Published thermochronologic data from the Qiangtang Basin come mainly from the Qiangtang culmination (Rohrmann *et al.*, 2012; Zhao *et al.*, 2017), and sparsely from detrital sandstones (Wang *et al.*, 2008a; Wang & Wei, 2013; Ren *et al.*, 2015). Cooling ages of different thermochronometers range from Early Jurassic to Cenozoic, and the initial timing of plateau growth is thought to range from Early Cretaceous to Paleogene (Wang *et al.*, 2008a; Rohrmann *et al.*, 2012; Zhao *et al.*, 2017).

Present-day stratigraphic thicknesses are the products of cumulative changes in rock volume through time caused by subsidence and burial (Allen & Allen, 2005). Reconstructing the subsidence histories of sedimentary basins provides **data** to directly interrogate the tectonic evolution of a basin (e.g. Brunet *et al.*, 2003; Carrapa & Garcia-Gastellanos, 2005; Abadi *et al.*, 2008; Holt *et al.*, 2010, 2015; Kuhn *et al.*, 2010; Sciunnach & Garzanti, 2012; Abdullayev *et al.*, 2017; Dressel *et al.*, 2017; Silvia *et al.*, 2017; Tozer *et al.*, 2017). The most commonly applied method to recover the 1-D subsidence history of a sedimentary basin is “backstripping” (Watts & Ryan, 1976; Sclater & Christie, 1980), which relies on physical properties of **the**

1
2
3
4
5
6
7
8
9
10
11
12
13
14
15
16
17
18
19
20
21
22
23
24
25
26
27
28
29
30
31
32
33
34
35
36
37
38
39
40
41
42
43
44
45
46
47
48
49
50
51
52
53
54
55
56
57
58
59
60

89 stratigraphic sequences (thickness and porosity), combined with depositional ages,
90 paleobathymetry and eustasy at the time of accumulation. The exhumation of
91 sedimentary basins is usually related to tectonic evolution, surface erosion and deep
92 geological processes (Bernet *et al.*, 2001; Reiners & Brandon, 2006). Various
93 thermochronometric systems have been used to provide important information on the
94 timing and duration of cooling events that can be related to rock uplift and erosion of
95 a sedimentary basin (Naeser *et al.*, 1989; Cederbom *et al.*, 2004; Armstrong, 2005).

96 This study carried out subsidence analysis of the Mesozoic Qiangtang Basin
97 using stratigraphic successions obtained from geological surveys during the last three
98 decades. New subsidence curves of the Qiangtang Basin established in this study
99 suggest a transition from a foreland basin on the south of the JRSZ during Triassic
100 times, to a hinterland basin (Horton, 2012) from Middle Jurassic to Early Cretaceous
101 times. The cooling history of the basin is constrained using apatite fission track data
102 from sandstones with modelling results indicating Early Cretaceous basin inversion
103 and exhumation, which we interpret to be related to the collision of the Amdo
104 basement or the initial amalgamation between the Lhasa and Qiangtang terranes. Our
105 results contribute to the understanding of the evolution of the Qiangtang Basin and
106 have implications for the Mesozoic growth of the Tibetan plateau.

107 **GEOLOGIC BACKGROUND**

108 The Tibetan plateau consists of several tectonic terranes, including the
109 Himalayas, Lhasa, Qiangtang, Songpan-Ganze, and Kunlun-Qaidam, divided by
110 several nearly east-west suture zones (Yin & Harrison 2000; Dai *et al.*, 2011; Zhang

111 *et al.*, 2012). The Qiangtang terrane, located in the central part of the plateau, is
 112 delimited by the JRSZ to the north and the BNSZ to the south (Fig. 1a). The JRSZ is
 113 considered to represent the closure of the Palaeo-Tethys Ocean in Permian to Late
 114 Triassic times, which opened probably in Early Carboniferous or earlier (Dewey *et al.*,
 115 1988; Pearce & Houjun, 1988; Kapp *et al.*, 2003; Zhai *et al.*, 2015). Middle to Upper
 116 Triassic deep-marine turbidites derived from surrounding blocks are preserved in the
 117 triangle-shaped Songpan-Ganze terrane north of the JRSZ (Nie *et al.*, 1994; Weislogel
 118 *et al.*, 2006; Ding *et al.*, 2013a). The Songpan-Ganze terrane was strongly deformed
 119 in the Late Triassic during closure of Paleo-Tethys (Chang, 2000; Roger *et al.*, 2011).
 120 Meanwhile, suturing along the JRSZ had taken place by Late Triassic (Norian) times,
 121 supplying a source of sediment southwards to the Qiangtang Basin (Li *et al.*, 2003).
 122 New geophysical and geochemical evidence reveal that the Songpan-Ganze complex
 123 may have subducted southward beneath the Qiangtang terrane along the JRSZ during
 124 Late Triassic (Zeng *et al.*, 2015; Lu *et al.*, 2017).

125 The BNSZ represents the closure of the Meso-Tethyan seaway along the
 126 southern margin of the Qiangtang terrane during Late Jurassic to Late Cretaceous
 127 times, resulting in amalgamation of the Lhasa and Qiangtang terranes (Fig. 1a) (Yin &
 128 Harrison, 2000; Kapp *et al.*, 2007; Zhu *et al.*, 2013, 2016; Fan *et al.*, 2015; 2016; Li *et*
 129 *al.*, 2016; Yan *et al.*, 2016; Chen *et al.*, 2017a; Huang *et al.*, 2017; Li *et al.*, 2017a;
 130 Liu *et al.*, 2017). Ophiolite fragments and Mesozoic clastic units (Li *et al.*, 2017b)
 131 within the BNSZ are tectonically superimposed. The Amdo basement (Fig. 1b) may
 132 have been isolated as a microcontinent or a continental arc during the formation of the

1
2
3
4
5
6
7
8
9
10
11
12
13
14
15
16
17
18
19
20
21
22
23
24
25
26
27
28
29
30
31
32
33
34
35
36
37
38
39
40
41
42
43
44
45
46
47
48
49
50
51
52
53
54
55
56
57
58
59
60

133 Bangong-Nujiang Meso-Tethyan Ocean ophiolites (Guynn *et al.*, 2006; Zhang *et al.*,
134 2014).

135 The Qiangtang Basin is subdivided into the North Qiangtang sub-basin, the
136 Central Uplift, and the South Qiangtang sub-basin (Fig. 1b, Wang *et al.*, 2004b). The
137 Central Uplift is composed of blueschist-bearing metamorphic *mélange* (Kapp *et al.*,
138 2000; Zhang *et al.*, 2006; Pullen & Kapp, 2014), Paleozoic low-grade strata (Kapp *et*
139 *al.*, 2000), and Late Triassic intermediate to felsic intrusive rocks (Kapp *et al.*, 2000;
140 Li *et al.*, 2015a). The contacts between metamorphic rocks and overlying
141 Paleozoic-Triassic low-grade strata are low-angle normal faults (Kapp *et al.*, 2000,
142 2003). The formation of the Central Uplift is still an enigma, with interpretations
143 ranging from an in-situ suture (Longmucuo-Shuanghu suture zone, LSSZ) (e.g., Li *et*
144 *al.*, 1995; Zhang *et al.*, 2006; Liu *et al.*, 2011; Zhao *et al.*, 2014, 2015; Zhai *et al.*,
145 2015; Yan *et al.*, 2016; Liang *et al.*, 2017) to the underthrust model that the *mélange*
146 was thrust beneath the Qiangtang terrane from the north and exhumed to the surface
147 by large-scale core complexes (e.g., Yin & Harrison, 2000; Kapp *et al.*, 2000, 2003;
148 Pullen & Kapp, 2014).

149 Despite the fact that the tectonic significance of the Central Uplift is debated, the
150 Mesozoic stratigraphic sequences in both the North and South Qiangtang are well
151 documented. In the North Qiangtang region they are separated by two major
152 unconformities in **Upper** Triassic to **Lower** Jurassic and the **Lower** Cretaceous; while
153 in the South Qiangtang region, the Mesozoic strata are complete until the **Lower**
154 Cretaceous (Fig. 2). Lower and Middle Triassic strata are sparse throughout the entire

Qiangtang Basin. **Upper** Triassic sediments are represented by offshore to shallow marine limestones (Juhuashan Fm. of the North Qiangtang), deep marine **flysch** (Zangxiahe Fm.), and **deltaic** and littoral sandstones, siltstones and mudstones (Riganpeicuo Group of the South Qiangtang). The Nadigangri volcanic rocks overlie the paleo-weathering crusts in some places in the North Qiangtang (Fu *et al.*, 2007; Wang *et al.*, 2007). This set of volcanic rocks was considered to record the onset of filling of the Mesozoic Qiangtang Basin (Wang *et al.*, 2004b; Fu *et al.*, 2010), and assigned to an Early Jurassic (Zhu *et al.*, 1996, 1997) or Middle Jurassic age (Wang *et al.*, 2001) until Zhai & Li (2007), Wang *et al.* (2008b) and Fu *et al.* (2010) presented SHRIMP zircon U-Pb ages of 219 ± 4 Ma, 216 ± 4.5 Ma and 220.4 ± 2.3 Ma, respectively.

The Jurassic sequences are complete in both the northern and southern portions of the Qiangtang Basin, except that the Lower Jurassic units are missing in the North Qiangtang, while contemporaneous sequences in the South Qiangtang are represented by coastal black shales interbedded with limestones and gypsum (Quse Fm., Fig. 2). The earliest Middle Jurassic successions include tidal or **deltaic** coarse sediments (Qumocuo Fm. of the North Qiangtang) and shallow-marine black shales with limestones (Sewa Fm. of the South Qiangtang) (Wang *et al.*, 2004b). The upper sequences of the Middle Jurassic consist of marine platform limestones, dolomites (Buqu Fm., Ding *et al.*, 2013b) and regressional semi-closed tidal flat sediments (Xiali Fm., Song *et al.*, 2017). The Upper Jurassic unit is represented by intra-platform littoral-neritic carbonate rocks and black shales deposited in a closed,

deep and static marine environment (Suowa Fm., Wang *et al.*, 2013).

During latest Jurassic to earliest Cretaceous **times**, the stratigraphic sequences are represented by clastic-carbonate sediments. The marine sedimentation in the North Qiangtang during **the** Early Cretaceous is represented by Xueshan Fm. and diachronous Bailongbinghe, Suowa and Xiali formations (Li & Batten, 2004; Yang *et al.*, 2017). Although Zhang (2000) and Zhang *et al.* (2004) asserted that the southern half of Qiangtang terrane was an area of marine sedimentation during Early Cretaceous, the marine sediments prevailed in its southern margin, close to the BNSZ. They have closer affinity to the BNSZ (Li *et al.*, 2017b) and are divided into different stratigraphic divisions (Mugagangri stratigraphic area) from the Jurassic sediments in the South Qiangtang. Overlying the repeated transgressive and regressive sequences (Ding *et al.*, 2013b) is **a Lower** Cretaceous unconformity. Upper Cretaceous alluvial and fluvial red sediments (Abushan Fm.) occupied the South Qiangtang depression, but are not found in its northern counterpart (Fig. 2). Its age has been defined to 102-75 Ma (Late Cretaceous) by different geochronological methods (Li *et al.*, 2013; Wu *et al.*, 2014; Li *et al.*, 2015c; Chen *et al.*, 2017b). Cenozoic terrestrial deposits unconformably overlie these Upper Cretaceous sequences.

METHODS

Backstripping and Data

The principle of backstripping analysis is an inverse modelling approach utilizing the stratigraphic record (Watts & Ryan, 1976; Sclater & Christie, 1980). Both the total and backstripped subsidence curves are time versus depth diagrams. In

1
2
3
4 199 the actual operating process, the first step is stratigraphic correlations and age
5
6 200 assessment, after which combining decompaction, palaeobathymetry and eustasy
7
8
9 201 yield the total subsidence history. By removing the subsidence generated by sediment
10
11 202 and water loads, the component of subsidence driven by tectonic forcing remains
12
13
14 203 (Magoon & Dow, 1994; Stapel *et al.*, 1996). We used a MATLAB program (Yao *et*
15
16 204 *al.*, 2017) to calculate the final tectonic subsidence and error bars.

205 Stratigraphic units

206 An issue is the poor exposure of the stratigraphic successions in the Qiangtang
207 Basin where strong weathering and Cenozoic deformation (Kapp *et al.*, 2005) affect
208 preservation. All the exploration wells, currently, are shallow ones (none deeper than
209 1.5 km) that encounter only a small part of the Mesozoic successions. Therefore,
210 subsidence recovery was accomplished using surface sections. Geological survey
211 institutes from China and our working group have measured up to 235 detailed
212 stratigraphic sections in the Qiangtang Basin. The first step is integrating scattered
213 sections into a composite successive column by lithologic or biostratigraphic
214 correlations (Sciunnach & Garzanti, 2012). As many measured stratigraphic sections
215 are hard to be integrated into one composite profile, because of the incomplete
216 exposure of Mesozoic sequences in one depression or severe disturbance caused by
217 Cenozoic deformation, we managed to restore eleven composite profiles in total (see
218 the Supporting information for the GPS data of all 235 sections and precise locations
219 of 11 composite profiles on Google Earth). For each of the eleven selected composite
220 sections, the average thickness of the various sections was used among the numerous

1
2
3
4
5
6
7
8
9
10
11
12
13
14
15
16
17
18
19
20
21
22
23
24
25
26
27
28
29
30
31
32
33
34
35
36
37
38
39
40
41
42
43
44
45
46
47
48
49
50
51
52
53
54
55
56
57
58
59
60

221 profiles in the same depression. The details of thickness of each stratigraphic unit are
222 given in Table S1.

223 In the North Qiangtang, nine locations were chosen to conduct subsidence
224 analyses, partly because the North Qiangtang occupies a large portion of the basin
225 (Fig. 1). Most locations have disrupted sequences, except for Nadigangri and Quemo
226 Co (Fig. 3). Three major unconformities can be found in strata exposed in the North
227 Qiangtang (Figs. 2 and 4). All of the sections, at the bottom, are characterized by
228 Upper Triassic marine limestones (Juhuashan Fm. of Duxue Mt., Shuangquan Lake,
229 and Zuerkenwula Mt., and Bolila Fm. of Quemo Co), and clastic deposits (Zangxiahe
230 Fm. of Heihuling and Changshui River, Tumengela Group of Dangmagang, and
231 Bagong Fm. and Erlongba Fm. of Quemo Co), with the exception of the Nadigangri
232 and Amugang sections which do not preserve marine deposits. The Amugang section
233 is represented by Permian metavolcanic rocks which underlie the whole sequence.
234 The first major gap appears between the marine deposits and overlying volcanic rocks
235 (Nadigangri Fm.). This unconformity appears only in the western part of the North
236 Qiangtang (Duxue Mt., Shuangquan Lake, Heihuling and Nadigangri), while the
237 eastern portion only exhibits the second major unconformity, which is prevalent
238 across the North Qiangtang. The second major unconformity is between Upper
239 Triassic and Middle Jurassic strata. The Lower Jurassic units are missing in the North
240 Qiangtang, suggesting a long-term hiatus or tectonic uplift after the closure of Jinsha
241 River suture to the north. The Middle Jurassic successions include Qumocuo Fm.,
242 Buqu Fm. and Xiali Fm. (Fig. 4). The Upper Jurassic unit is represented by Suowa

243 Fm. During latest Jurassic to earliest Cretaceous, the stratigraphic sequences consist
244 of clastic sediments, Bailongbinghe and Xueshan formations (Fig. 2). Note that the
245 Bailongbinghe and Xueshan formations are probably contemporaneous heterotopic
246 facies so that they are not both recorded in some locations. The last major
247 unconformity is between Cenozoic fluvial and lacustrine Kangtuo Fm. and latest
248 Jurassic to earliest Cretaceous sandstones. No Late Cretaceous sediments were
249 discovered.

250 Two sites were considered ideal for modelling of subsidence histories of the
251 South Qiangtang, the Biluo Co and Dazhuoma sections (Figs. 1 and 5). Mesozoic
252 sequences are more complete than that of the North Qiangtang, with only one or two
253 major unconformities recognized (Fig. 5). The Late Triassic sequences are
254 represented by fine-grained clastic deposits (Riganpeico Group of Biluo Co and Adula
255 Fm. of Dazhuoma), sandstones (Duogaila Fm. of Dazhuoma), and limestones
256 (Suobucha Fm. of Biluo Co). It is noticeable that the Biluo Co section is complete,
257 while the Dazhuoma section has an obvious unconformity between the Jurassic
258 Quemocuo Fm. and the Triassic sandstones. This indicates an east-west difference in
259 the paleogeography of the South Qiangtang. The early stage of the Jurassic sequences
260 seems to record contemporaneous heterotopic facies in Biluo Co (Quse Fm. and Sewa
261 Fm.) and Dazhuoma (Quemocuo Fm.), respectively. The discrepancy lies in the grain
262 size and thickness where the Biluo Co section is finer and thicker (Fig. 5). The rest of
263 the Jurassic sequences are characterized by limestones interbedded with sandstones,
264 siltstones and mudstones. The lower limestone unit, Buqu Fm., preserves dolomites

1
2
3
4
5
6
7
8
9
10
11
12
13
14
15
16
17
18
19
20
21
22
23
24
25
26
27
28
29
30
31
32
33
34
35
36
37
38
39
40
41
42
43
44
45
46
47
48
49
50
51
52
53
54
55
56
57
58
59
60

and gypsum, reflecting an arid period during a marine transgression-regression cycle.

The upper limestone unit, Suowa Fm., is characterized by darker bioclastic limestone.

The interbedded clastic unit is relatively fine grained. A regional unconformity appears above the upper limestone unit, with latest Jurassic to earliest Cretaceous clastic deposits missing in the South Qiangtang compared to that of the North Qiangtang (Figs. 4 and 5). The Late Cretaceous Abushan Fm. is only recognized in the South Qiangtang, which is unconformably overlain by Cenozoic Kangtuo Fm.

Age constraints

Hundreds of samples from regional geological surveys were studied for biostratigraphy (e.g., ammonoids, bivalves, corals, brachiopods, foraminifers, radiolarians, fusulinids, etc., see Table S2 in Supporting material for details about fossils and their constrained biostratigraphy), resulting in reliable biostratigraphic control (e.g., Chen *et al.*, 2016; Yin, 2016; Yin & Chandler, 2016) and refined palaeoenvironmental and palaeowater-depth interpretations. All Jurassic strata contain abundant bivalves to constrain ages (Table 1). In addition, ages of Jurassic sequences are constrained by magnetostratigraphy of Fang *et al.* (2016) (Fig. 2).

The accuracy of subsidence history plots heavily depends on the precision of age assessment. The choice of timescale is important when transforming relative ages derived from biostratigraphy into numerical ages. However, there are a few differences in recent timescales by different authors, and so we adopt the standard timescale of Gradstein *et al.* (2004) and Ogg *et al.* (2008).

Decompaction

The quantitative analysis of total subsidence history relies mainly on stepwise decompaction of stratigraphic units (Bond & Kominz, 1984). The principle of decompaction is based on the reduction of porosity with depth (Allen & Allen, 2005 and references therein). Generally the porosity decreases exponentially with depth (Steckler & Watts, 1978; Sclater & Christie, 1980):

$$\Phi = \Phi_o e^{-cy} \quad (1)$$

where Φ_o is the surface porosity, Φ is the porosity at the given depth y , and c is a lithology-dependent coefficient. The standard Φ_o and c values for different lithologies used in this study come from Sclater & Christie (1980).

In the decompaction process, when recovering the depths y_1 and y_2 of the sedimentary unit to its initial uncompacted depths y_1' and y_2' (Fig. 6), the decompacted thickness H , will be the following result (Allen & Allen, 2005):

$$H = y_2' - y_1' = y_2 - y_1 + \Phi_o [(e^{-cy_1'} - e^{-cy_2'}) - (e^{-cy_1} - e^{-cy_2})] / c \quad (2)$$

where $\Phi_o(e^{-cy_1'} - e^{-cy_2'})/c$ is the pore volume after decompaction, and $\Phi_o(e^{-cy_1} - e^{-cy_2})/c$ is the pore volume before **decompaction**.

Backstripping

The total subsidence is divided into two parts, one resulting from the tectonic driving forces and the other caused by sediment and water loads. The subsidence

1
2
3
4
5
6
7
8
9
10
11
12
13
14
15
16
17
18
19
20
21
22
23
24
25
26
27
28
29
30
31
32
33
34
35
36
37
38
39
40
41
42
43
44
45
46
47
48
49
50
51
52
53
54
55
56
57
58
59
60

curve obtained after decompaction is the total subsidence (Watts *et al.*, 1982; Busby & Ingersoll, 1995). Sediment load must be subtracted by means of isostatic models (Einsele, 1992). An Airy isostastatic model was adopted in this study.

In an Airy isostastatic model, the tectonic subsidence, D , can be backstripped from H using the equation given by Watts & Ryan (1976):

$$D=H(\rho_m-\rho_s)/(\rho_m-\rho_w) \tag{3}$$

where ρ_m , ρ_s , and ρ_w are densities of lithospheric mantle, sediments and water, respectively. Values for ρ_m and ρ_w are constant and we adopt 3.33 and 1.035 g/cm³ for each of them. Values for ρ_s are calculated in terms of weighted mean average densities of different lithologies during progressive decompaction using the following equation (Allen & Allen, 2005):

$$\rho_s=\Sigma\{[\Phi_i\cdot\rho_w+(1-\Phi_i)\rho_{sgi}]/H\}Y_i' \tag{4}$$

where Φ_i is the porosity of a specific layer, ρ_{sgi} is the sediment grain density of one layer, and Y_i' is the thickness of layer i .

Boundary conditions

Sea-level changes and paleo-water depths are usually used as boundary conditions in modelling. Although regional sea-level changes often differ from global scales, global sea-level curves are used in many cases. We adopt the eustatic sea-level

curves of Miller *et al.* (2005) for Mesozoic eustatic corrections. The eustasy data are given in Table S1.

Paleo-water depth often has a wide range of uncertainty (e.g., Bertram & Milton, 1988) and are derived primarily from fossils, sedimentary structures, geochemical signatures (values and ratios of trace, transition and rare earth element, etc.), and depositional environment interpretations (Sciunnach & Garzanti, 2012) (Fig. 7). For instance, the biomarkers of the Middle Jurassic Buqu Formation indicate an offshore to shallow marine environment (Chen *et al.*, 2014), which suggested a paleo-water depth of 0-150 m. All the paleo-water depths used in the modelling are listed in Table S1 in Supplementary material.

After corrections for paleo-water depth and variations in sea-level change are conducted, the Airy compensated tectonic component of basement subsidence, Y , is (Sclater & Christie, 1980):

$$Y = D + W_d - \Delta_{sl} \cdot \rho_m / (\rho_m - \rho_w) \quad (5)$$

where W_d is the assumed paleo-water depth, and Δ_{sl} is paleo-sea level relative to the present.

The uncertainties of backstripping methods

Generally, the uncertainty of stratigraphic thickness is small. It mostly comes from the unknown amount of erosion at unconformities. The apatite fission track analyses could constrain the erosion thickness in the Dazhuoma section (Figs. 1 and 5;

1
2
3
4
5
6
7
8
9
10
11
12
13
14
15
16
17
18
19
20
21
22
23
24
25
26
27
28
29
30
31
32
33
34
35
36
37
38
39
40
41
42
43
44
45
46
47
48
49
50
51
52
53
54
55
56
57
58
59
60

Table 2). However, it can not be applied to the other sections. As a result, this correction was neglected, as assessment of the amounts of erosional removal are not accessible in these sections; it is recognized that this provides uncertainty in the final subsidence calculation.

Age assessment has a large uncertainty because most of the age constraints derive from biostratigraphy. Only the volcanic rocks of Late Triassic Nadigangri Fm. are constrained by U-Pb zircon dating. The uncertainty in age assessment causes little change to the shape of subsidence curves. The biostratigraphy information of all the sequences are tabulated in Table S2 in Supplementary material.

Paleo-water depth often has a wide range of uncertainty, especially for deep-water units (Sciunnach & Garzanti, 2012). In our study, paleo-water depths are based on the interpretation of paleo-environment and have large errors on them. Sea-level corrections are based on curves generated from the Atlantic passive margin (Miller *et al.*, 2005), which may differ from regional sea-level histories linked to variations in the geoid.

Finally, the use of a simple Airy isostatic correction is applied as there is uncertainty around the flexural rigidity of the plate during the Mesozoic loading. The implication is that the rates of tectonically induced subsidence following backstripping would have been greater, but the pattern of subsidence unchanged (Allen and Allen, 2005).

Apatite Fission Track Thermochronology

Materials and methods

12 sandstone samples were collected for apatite fission track (AFT) analyses (Fig. 1; GPS coordinates are given in Table S3 in Supplementary material). Seven samples came from the Amugang, Biluo Co and Dazhuoma sections (Figs. 4 and 5). The other five were from geological surveys. Fission track ages, track lengths, and D_{par} (etched pits of fission tracks on a polished surface) measurements were performed at the University of Glasgow using the external detector method (Gleadow, 1981; Donelick *et al.*, 2005) and the zeta calibration technique (Huford & Green, 1983), following the techniques provided by Persano *et al.* (2005). Apatite grains were etched for 20 s in 5.0 M HNO_3 at room temperature ($\sim 20^\circ C$). Mica detectors were etched with HF for 25 min. Samples were irradiated at Oregon State TRIGA Reactor, USA. Apatites were irradiated together with IRMM 540R dosimeter glasses to check the constancy of the neutron flux. The samples and standards were counted under a Carl Zeiss Axio Imager M1m optical microscope at $1250 \times$ magnification and the FTStage 4.04 system by Trevor Dumitru. All AFT data were processed and plotted using TrackKey software (Dunkl, 2002); their populations were analyzed using Density Plotter (Vermeesch, 2012). The χ^2 test (Galbraith, 1981; Green, 1981) was performed on all samples to determine the populations in a grain-age distribution.

Thermal History Modelling

HeFTy, a Monte Carlo approach to data interpretation (Ketcham *et al.*, 2005), was used to decipher thermal history. Fission track age and track length were modelled using the multi-kinetic annealing model of Ketcham *et al.* (2007), using D_{par} as a kinetic parameter (Donelick *et al.*, 2005). Inverse thermal history modelling

1
2
3
4
5
6
7
8
9
10
11
12
13
14
15
16
17
18
19
20
21
22
23
24
25
26
27
28
29
30
31
32
33
34
35
36
37
38
39
40
41
42
43
44
45
46
47
48
49
50
51
52
53
54
55
56
57
58
59
60

was run until 100 good paths were obtained, which in all cases resulted >10000 acceptable paths.

RESULTS

Subsidence History

Subsidence history of the nine locations in the North Qiangtang and two in the South Qiangtang were generated (Fig. 8). A total decompacted subsidence curve and a backstripped, tectonic subsidence curve were obtained for each site.

All curves of the North Qiangtang show two stages of concave-up subsidence, a lower magnitude during Late Triassic and a more pronounced stage during Middle Jurassic to Early Cretaceous. In the first stage, rapid tectonic subsidence was recorded during middle Late Triassic, followed by a deceleration or termination in tectonic subsidence. To more clearly understand the latter stage of subsidence history, we focus on the subsidence curves from ~172 Ma to 120 Ma (Fig. 9). This stage of subsidence started at around 172 Ma, with subsidence curves that are either concave or nearly linear (e.g., Duxue Mt. and Shuangquan Lake). The last phase of most subsidence curves decelerate with time with the exception of Duxue Mt. and Shuangquan Lake (Fig. 9). A suspension was recorded in the Heihuling profile at about 165 Ma.

Two sites in the South Qiangtang show distinct subsidence patterns. The subsidence rate of Biluo Co accelerated with time at first, and then decelerated in the Late Jurassic (Fig. 8). In contrast, the subsidence curve of Dazhuoma shows a two-stage evolution, which is similar to those in the North Qiangtang.

419 **Apatite Fission Track**

420 Central ages of all sandstone samples range from 120.9 ± 5.5 to 40.1 ± 2.6 Ma
 421 (Table 2), which are much younger than the stratigraphic ages (Triassic-Cretaceous).
 422 The grain-age distributions can be divided into two groups. One is late Early to Late
 423 Cretaceous (120.9-84.1 Ma) and another is Paleogene-Eocene (65.4-40.1 Ma). Four
 424 samples (ED0616, EP1502, EP1504-17 and PQ1503) failed the χ^2 test, suggesting that
 425 the apatite composition may vary significantly within each sample (O'Sullivan &
 426 Parrish, 1995) and they may have multiple age populations. The age dispersion of
 427 these four samples are moderate to high ($> 20\%$) (Table 2). Despite failing the χ^2 test,
 428 a mixture model (Galbraith & Green, 1990) does not show two populations for the
 429 majority of samples, with exception of sample EP1502 (Fig. 10). The relatively short
 430 mean horizontal confined track lengths (MTLs) range from 9.26 ± 0.39 to $13.75 \pm$
 431 $0.48 \mu\text{m}$ (Table 2). This pattern suggests that these samples were buried within the
 432 partial annealing zone of AFT, or reheated for a long time before exhumed to the
 433 surface. Most samples have limited amount of horizontal confined tracks. Therefore,
 434 it is difficult to extract useful information from MTLs. D_{par} values range from 1.74 to
 435 $3.49 \mu\text{m}$, with many incomparable with Durango apatite ($2.05 \pm 0.16 \mu\text{m}$, Sobel &
 436 Seward, 2010), which means many samples have different compositionally controlled
 437 annealing properties compared with Durango apatite. The relatively large D_{par} values
 438 reflect the high values of Cl wt% ($> 1\text{-}2 \text{ wt}\%$, Donelick *et al.*, 2005 and references
 439 therein) in these samples, which suggests relatively slow annealing of apatite grains
 440 (Donelick *et al.*, 2005; Galbraith, 2005).

Thermal History Modelling

Three initial constraints were applied to four sandstone samples that were selected to run modelling: (1) temperature of 5 ± 5 °C for the present surface; (2) temperature of 20 ± 20 °C for the depositional ages, which were constrained by magnetostratigraphy of Fang *et al.* (2016); (3) temperature of 120-200 °C between 160-120 Ma, which is constrained by subsidence history, adopting a geothermal gradient of 30 °C/km (He *et al.*, 2014). Modelling results of four samples (ED0616, EP1502, PQ1503 and PQ1506) from the Qiangtang Basin indicate a relatively simple cooling history (Fig. 11; see Figure S1 for all thermal history models). After deposition, all samples reached maximum temperature 150-170 °C at about 150-130 Ma, which is much higher than the base of the apatite partial annealing zone (110 ± 10 °C, Ketcham *et al.*, 1999), suggesting entire reset apatite fission track ages. Cooling started at about 140-130 Ma, which is coincident with the timing of crustal thickening inferred from the subsidence history. After *ca.* 100 Ma, all the samples present protracted cooling histories, followed by increase in cooling rates, up to 2-5 °C Myr⁻¹, at *ca.* 25-10 Ma.

DISCUSSION

Subsidence Analyses of the Mesozoic Qiangtang Basin

Based on the subsidence histories (Figs. 8 and 9) combined with previous work on sediment provenance (Fig. 12) and timing of deformation, we suggest that the evolution of the Mesozoic Qiangtang Basin can be subdivided into two main stages, Late Triassic-Early Jurassic and Middle Jurassic-Early Cretaceous.

463 Late Triassic-Early Jurassic

464 The North and South Qiangtang may have been separated by the paleo-Tethys
465 Ocean before the Triassic (Li *et al.*, 1995; Song *et al.*, 2017). The North Qiangtang
466 was a foreland basin in the early Late Triassic to the south of the JRSZ (Li *et al.*, 2003;
467 Song, 2012), which resulted from the collision between the Songpan-Ganze and
468 Qiangtang (Yan *et al.*, 2016) (Fig. 13a). Li *et al.* (2003) proposed that the main
469 paleo-current directions at the northern edge of the North Qiangtang region were
470 southwestward, and the turbidites and delta sandstones transitioned to thinner and
471 finer foredeep sediments from north to south when marine Juhuashan and Zangxiahe
472 formations were deposited. Additionally, the Carnian mudstones were deposited under
473 a collisional setting based on the multi-major elements discriminate plots (Wang *et al.*,
474 2017a). The subsidence history patterns of the North Qiangtang are concave-upward
475 during early Late Triassic (grey-shaded area in Fig. 8), which is consistent with the
476 characteristics of subsidence curves of retro-foreland basins (Naylor & Sinclair, 2008),
477 though the subsidence is not remarkable and the error bars may make the data less
478 reliable. We interpret that the marine deposits in the North Qiangtang were generated
479 from flexural subsidence by orogenic loading in the JRSZ in the early Late Triassic
480 (Fig. 13a).

481 Provenance analyses and paleo-current directions indicate that the JRSZ had
482 been a topographic highland and source area by the end of Late Triassic when the
483 Nadigangri volcanic rocks formed (Li *et al.*, 2003). The presence of paleo-weathering
484 crusts (Fu *et al.*, 2007; Wang *et al.*, 2007), marking the termination of early Late

1
2
3
4
5
6
7
8
9
10
11
12
13
14
15
16
17
18
19
20
21
22
23
24
25
26
27
28
29
30
31
32
33
34
35
36
37
38
39
40
41
42
43
44
45
46
47
48
49
50
51
52
53
54
55
56
57
58
59
60

Triassic subsidence, means that the North Qiangtang was subaerially exposed in the Late Triassic. The Nadigangri volcanic rocks (~216-220 Ma) unconformably overlay the paleo-weathering crusts after the early Late Triassic subsidence ceased. The majority of these volcanic rocks are felsic, rather than basaltic. As a result, we interpret these, like other bimodal magmatism found in the North Qiangtang (Zhang *et al.*, 2011), to be a result of the detachment and sinking of oceanic lithosphere of the South Qiangtang in the Late Triassic (Zhai & Li, 2007; Zhai *et al.*, 2013) (Fig. 13b), but not as the onset of a rift basin (e.g., Fu *et al.*, 2010). The tectonic subsidence that accommodated the Nadigangri volcanic rocks (Fig. 8) is interpreted as subsidence due to local lithospheric stretching based on geochemical analyses of Fu *et al.* (2010). The North Qiangtang had been an area of erosion since the paleo-weathering crusts formed and it exhibits unconformities lasting about 50 m.y. on the tectonic subsidence curves (Fig. 8).

Although the large error bars also makes the data less reliable, the accelerating subsidence curve of Biluo Co in the South Qiangtang shows a unique characteristic of collisional **pro-foreland** basins (Kneller, 1991; Miall, 1995; DeCelles & Giles, 1996; Naylor & Sinclair, 2008) (Fig. 8). One possible explanation is that it evolved on the south of the Central Uplift mountain belt as the South Qiangtang collided with the North Qiangtang. (Li *et al.*, 1995; Liu *et al.*, 2011; Zhao *et al.*, 2014, 2015; Yan *et al.*, 2016; Liang *et al.*, 2017) (Fig. 13a). The convex-upward tract of the subsidence curve for Biluo Co demonstrates that local forces, the **northward** subduction of the South Qiangtang lithosphere and the growth of Central Uplift, probably played an important

507 role in controlling the development of the basin, just as other collisional foreland
 508 basins worldwide (e.g., North Alpine **Foreland Basin** of Homewood *et al.* (1986) and
 509 Ebro basin of Vergés *et al.* (1998)). New geochronology shows that the
 510 metamorphism in Central Uplift occurred at about 243-233 Ma (Pullen *et al.*, 2008;
 511 Dan *et al.*, 2018), marking the collision between the South and North Qiangtang.
 512 Subsequent exhumation occurred at 220-202 Ma (Kapp *et al.*, 2003; Dan *et al.*, 2018),
 513 which was synchronous with the commencement of subsidence at Biluo Co.
 514 Therefore, Late Triassic subsidence **in the western part of South Qiangtang** is
 515 interpreted to be caused by orogenic loading from the Central Uplift and static loads
 516 from the slab pull (Figs. 13a, b). However, **in the east**, the Dazhuoma site in the South
 517 Qiangtang shows a concave pattern of subsidence, which is similar to that of the
 518 North Qiangtang (Fig. 8). This suggests that there is a significant difference in basin
 519 evolution **between east and west portions of** the South Qiangtang during this time
 520 interval. In the eastern part (Dazhuoma), the Central Uplift was not created (Figs. 13a,
 521 b) and we interpret the subsidence arose from dynamic subsidence. As the shallowly
 522 subducting Paleo-Tethyan oceanic slab approached the South Qiangtang in the eastern
 523 part (Lu *et al.*, 2017), it **potentially** caused viscous mantle flow that **drove** the
 524 subsidence (Fig. 13a). **We ascribe differences between the eastern and western**
 525 **portions of** South Qiangtang to the irregular shape of continental margin (Zhang &
 526 Tang, 2009) and varying subducting angles of Paleo-Tethyan oceanic slab (Lu *et al.*,
 527 2017) (Fig. 13a).
 528 Middle Jurassic-Early Cretaceous

1
2
3
4
5
6
7
8
9
10
11
12
13
14
15
16
17
18
19
20
21
22
23
24
25
26
27
28
29
30
31
32
33
34
35
36
37
38
39
40
41
42
43
44
45
46
47
48
49
50
51
52
53
54
55
56
57
58
59
60

529 The Middle Jurassic to Early Cretaceous is the main period of subsidence in the
530 Mesozoic Qiangtang Basin. The Qiangtang terrane had been entirely accreted onto the
531 southern margin of Eurasia since Early Jurassic (Dewey *et al.*, 1988; Pearce & Houjun,
532 1988). The Central Uplift has been an area of active exhumation based on provenance
533 analysis and tectonic analyses (Li *et al.*, 2001; Kapp *et al.*, 2003) (Fig. 12). In addition,
534 the denudation of the ultrahigh-pressure (UHP) metamorphic rocks in the Central
535 Uplift is associated with lithospheric detachment and associated orogenic collapse
536 (Zhang & Tang, 2009) (Fig. 13c). The thrust belt loading from both the south and
537 north sides of the North Qiangtang potentially resulted in renewed subsidence. In
538 addition, the northward subduction of Bangong-Nujiang oceanic lithosphere during
539 180-150 Ma (Liu *et al.*, 2017) may have resulted in viscous corner flow beneath the
540 North Qiangtang (Fig. 13c). The subsidence started at around 172 Ma, and the rapid
541 subsidence of Duxue Mt. and Shuangquan Lake (Fig. 9) may have resulted from
542 additional sediments supply from the Central Uplift (Figs. 1 and 12).

543 The subsidence patterns resemble exponentially decaying thermal subsidence
544 curves formed in extensional settings (Steckler & Watts, 1978; Christie-Blick &
545 Biddle, 1985) and retro-foreland basins (Naylor & Sinclair, 2008; Sinclair & Naylor,
546 2012), or are associated with hinterland basins that show fast subsidence in very short
547 time interval (Horton, 2018). Such a high rate of subsidence generated through
548 extension would require β values to be over 2 (assuming homogeneous lithospheric
549 extension of a 33 km thick crust), which would have generated oceanic lithosphere
550 (Kneller, 1991), but no evidence is recorded. Moreover, no evidence of extensional

structures was found during Middle Jurassic to Early Cretaceous, such as syndepositional normal faults. Currently, all the discovered normal faults in central Tibet formed in Cenozoic times (e.g., Blisniuk *et al.*, 2001; Wang *et al.*, 2010; Ou *et al.*, 2017). In addition, no volcanic rocks, particularly basaltic rocks, are found in the Middle to Late Jurassic deposits. Therefore, we exclude lithospheric extension as the mechanism. Based on the subsidence histories combined with previous work on sediment provenance and timing of deformation, we prefer to interpret this stage of the North Qiangtang as a hinterland basin controlled by renewed crustal thickening, and loading from both the south and northern margins during Middle Jurassic-Early Cretaceous. This interpretation is supported by several lines of evidence. First, Li *et al.* (2001) reconstructed the paleogeomorphology and palaeogeography, based on paleo-current directions, composition of lithic fragments in sandstones and provenance analysis (Fig. 12). The molasses preserved in the Quemocuo Fm. (Fig. 4) represented the initiation of subsidence in the North Qiangtang. The composition of the overlying sandstones is consistent with deposition in a collisional setting in the light of multidimensional tectonic discrimination based on major element analysis (Wang *et al.*, 2017b). Sandstone modal analyses indicate the influx of sediments from a recycled orogen source (Li *et al.*, 2001). Combined with paleo-current directions, mainly southward and southwestward, the main source of the sediments must be the JRSZ to the north, and some detritus derived from the exhumation of tectonic culmination (the Central Uplift) in the basin (Fig. 12). In addition, the coarse sediments are distributed mainly along the edges of the North Qiangtang, suggesting

1
2
3
4
5
6
7
8
9
10
11
12
13
14
15
16
17
18
19
20
21
22
23
24
25
26
27
28
29
30
31
32
33
34
35
36
37
38
39
40
41
42
43
44
45
46
47
48
49
50
51
52
53
54
55
56
57
58
59
60

the tectonic loads on both sides were the main driving force for subsidence (Li *et al.*, 2001). Second, the thickness of marine sediments is 6-8 km in the north and 4-5 km in the south (Fig. 8). It means that there were other driving forces on the south to accommodate such thick sediments. This could occur in hinterland basins where there is thrust loading from both sides of the basin (Horton, 2012). Additional subsidence in the north may have been generated by dynamic loading, because it is where the corner flow drag is concentrated (Mitrovica *et al.*, 1989) (Fig. 13c). In addition, the flat subduction of Meso-Tethyan Ocean slab potentially transmitted strain in to the hinterland driving renewed crustal thickening, loading and marine transgression. Third, the average accumulation rate of sediments during this time was about 0.2 km/Ma, with some locations (Shuangquan Lake and Duxue Mt.) over 0.45 km/Ma. This accumulation rate is consistent with that obtained for the Buqu Formation at Well QZ11 (0.15-0.395 km/Ma with optimal value of 0.268 km/Ma, Cheng *et al.*, 2017). The high accumulation rates in a short time interval resemble those for Andean hinterland basins (Horton, 2018 and references therein). In summary, the subsidence of the North Qiangtang was controlled by the combined mechanisms of flexural subsidence from both the Jinsha River orogen and the Central Uplift and long-wavelength dynamic subsidence caused by northward shallow subduction of Meso-Tethyan Ocean lithosphere (Fig. 13c).

In the South Qiangtang, the subsidence curves show similar characteristics with the North Qiangtang during Middle Jurassic to Early Cretaceous times. The subsidence rates are also equal to those in the south of the North Qiangtang. We

interpret the subsidence in the South Qiangtang came from the subduction of Meso-Tethyan Ocean lithosphere and tectonic loading from the Central Uplift (Fig. 13c).

The deceleration in the last phase of subsidence might have resulted from the closure of the Bangong-Nujing Ocean or the onset of Lhasa-Qiangtang collision during Late Jurassic to Early Cretaceous (Yan *et al.*, 2016; Zhu *et al.*, 2016; Li *et al.*, 2017b). At about 148 Ma, subsidence terminated across the Qiangtang Basin. The beginning of exhumation of the Qiangtang Basin (Fig. 11) and the termination of subsidence happened simultaneously, probably indicating the onset of crustal thickening in the Qiangtang terrane.

Cretaceous

All subsidence curves in the North Qiangtang show the same trend with the Late Jurassic patterns that no subsidence is displayed (Fig. 8). No Late Cretaceous sediments are recorded. It was highly possible that the North Qiangtang started to show first stage of crustal thickening according to the thermal modelling results (PQ1503; Fig. 11).

The South Qiangtang records Late Cretaceous subsidence (Fig. 8). We interpret the Late Cretaceous Abushan Fm. as a response to the collision between Lhasa and Qiangtang terranes to the south (Yin & Harrison, 2000; Kapp *et al.*, 2007; Zhu *et al.*, 2013, 2016) (Fig. 13e), or to the collision of the Amdo terrane (Guynn *et al.*, 2006) (Fig. 13d). The oldest apatite fission track age (120.9 ± 5.5 Ma) may record the collision between the two terranes.

Implications for Pre-Cenozoic Evolution of the Tibetan Plateau

The timing of the topographic evolution of the Tibetan Plateau is still uncertain, though the general consensus is that central Tibet and surrounding areas had attained high elevation by 45 Ma or earlier (Murphy *et al.*, 1997; Kapp *et al.*, 2005, 2007; Rowley & Currie, 2006; Wang *et al.*, 2008a, 2014; Rohrmann *et al.*, 2012; Chen *et al.*, 2013; Xu *et al.*, 2013; Ding *et al.*, 2014; Tang *et al.*, 2017). Is the India-Asia collision strong enough to produce such high elevation and thickened crust in a very short period of time? The hinterland of the Tibetan plateau shows both a cessation of subsidence and an acceleration of exhumation recorded in zircon (U-Th)/He ages in the South Qiangtang (Zhao *et al.*, 2017) and apatite fission track modelling (Fig. 11), consistent with topographic growth at ca. 148 Ma. Mesozoic sediments were exhumed from >6 km depth at about 140-130 Ma, with exhumation rate of 0.1-0.3 mm/a (Fig. 11). This cooling event is also in agreement with accelerated cooling reflected by Late Jurassic-Cretaceous apatite fission ages from sedimentary rocks across the Qiangtang terrane (Wang & Wei, 2013; Ren *et al.*, 2015). This incident may mark the first stage of exhumation driven by crustal thickening in central Tibet (Zhao *et al.*, 2017). We ascribe the exhumation in central Tibet to the onset of continental collision between Lhasa and Qiangtang terranes, probably involving underthrusting of the Lhasa terrane beneath the Qiangtang terrane. Concurrent crustal thickening with collision suggests that the impact of the collision between Lhasa and Qiangtang terranes was potentially more profound than previously thought. The Jinsha River suture zone also played a role that can not be ignored, because both the Songpan-Ganze and Lhasa terranes may

1
2
3
4 639 have been involved in underthrusting beneath the Qiangtang terrane. Alternatively,
5
6 640 the Late Jurassic-Early Cretaceous exhumation (Fig. 11) or crustal thickening could
7
8
9 641 be related to collision of the Amdo terrane caused by northward continental
10
11 642 underthrusting of the Lhasa terrane (Guynn *et al.*, 2006) (Fig. 13d). The Amdo
12
13 643 basement was interpreted to be exposed only at the central part of BNSZ, but buried
14
15 644 in all other places (Guynn *et al.*, 2006). Recently, Li *et al.* (2017c) reported the
16
17 645 existence of a destroyed Amdo-Tongka block through study along the eastern segment
18
19 646 of BNSZ. Therefore, there may be an unrecognized block south of the Qiangtang
20
21 647 terrane. Both scenarios suggest that the underthrusting of the Lhasa terrane
22
23 648 contributed to the rapid exhumation or crustal thickening in central Tibet at about
24
25 649 150-130 Ma.

26
27 650 As shown in Figs. 8 and 9, the tectonic subsidence curves show no subsidence
28
29 651 since the beginning of the Cretaceous, with cessation of marine deposition. At this
30
31 652 time, the North Qiangtang started to record substantial crustal thickening and
32
33 653 increased elevations. Cretaceous apatite fission track ages (120.9-84.1 Ma) reflect
34
35 654 exhumation caused by a strong compressive episode (Rohrmann *et al.*, 2012; Ren *et*
36
37 655 *al.*, 2015). Large magnitudes of convergence after ~100 Ma were documented
38
39 656 between Lhasa and Qiangtang using paleomagnetic data (Chen *et al.*, 2017b), which is
40
41 657 coeval with protracted cooling histories (Fig. 11). This event slightly lagged behind
42
43 658 the closure of the BNSZ south of Qiangtang, which indicates that the crustal
44
45 659 thickening of central Tibet was a result of continued convergence between Lhasa and
46
47 660 Qiangtang. The cooling ages of Paleogene-Eocene (65.4-40.1 Ma) may reflect the
48
49
50
51
52
53
54
55
56
57
58
59
60

1
2
3
4
5
6
7
8
9
10
11
12
13
14
15
16
17
18
19
20
21
22
23
24
25
26
27
28
29
30
31
32
33
34
35
36
37
38
39
40
41
42
43
44
45
46
47
48
49
50
51
52
53
54
55
56
57
58
59
60

661 early impact of the India-Asia collision on the Qiangtang, which probably involved
662 underthrusting of greater Indian lithosphere as far north as the Qiangtang terrane
663 (Rohrmann *et al.*, 2012).

664 **CONCLUSIONS**

665 We have conducted backstripping of basin stratigraphy and thermochronological
666 analyses of Mesozoic sandstones to study the subsidence and exhumation of the
667 Qiangtang Basin. The results not only reveal the evolution of the Mesozoic Qiangtang
668 Basin, but also yield insight into the early growth of the Tibetan Plateau.

669 Based on the subsidence histories, combined with previous work on sediment
670 provenance, timing of deformation, and thermochronologic data, we suggest that the
671 evolution of the North Qiangtang sub-basin can be subdivided into two main stages.
672 The first stage is Late Triassic to Early Jurassic and the second is Middle Jurassic to
673 Early Cretaceous. In the early Late Triassic, the marine deposits were generated from
674 flexural subsidence by orogenic loading in the JRSZ. Whereas the Nadigangri
675 volcanic rocks were accommodated by thermal subsidence caused by local lithosphere
676 stretching during Late Triassic. During the second stage, the subsidence was
677 controlled by flexural subsidence from active shortening in the Central Uplift and the
678 southern edge of the Jinsha orogeny, combined with long-wavelength dynamic
679 subsidence caused by shallowly northward subduction of Meso-Tethyan Ocean
680 lithosphere. Both stages are characterized by concave-upward subsidence curves.
681 Initiation of exhumation reflected by thermal history modelling in the Early
682 Cretaceous, may represent crustal thickening in central Tibet.

The subsidence of the South Qiangtang sub-basin can also be subdivided into two stages. The first stage (Late Triassic-Early Jurassic) in the western part is represented by an accelerating pattern of subsidence, which is typical of a collisional pro-foreland basin. This was caused by orogenic loading from the Central Uplift and static loads from the slab pull. Whereas in the eastern part, the subsidence was interpreted to come from dynamic loading caused by viscous mantle flow. The second stage (Middle Jurassic-Early Cretaceous) was controlled by the subduction of Meso-Tethyan Ocean lithosphere and tectonic loading from the Central Uplift.

The cessation of tectonic subsidence curves and initiation of cooling indicated in the thermal modelling histories may represent the first stage of rapid exhumation or crustal thickening in central Tibet at about 150-130 Ma. The central part of the plateau had probably begun to accumulate substantial crustal thickening and elevation, probably driven by underthrusting of both the Lhasa and Songpan-Ganze terranes beneath the Qiangtang terrane, or the collision of the Amdo terrane. The growth of the Tibetan Plateau may have begun before the India-Asia collision.

ACKNOWLEDGEMENTS

We acknowledge Dr. Nadine McQuarrie, Dr. Alexander Robinson, Dr. Paul Kapp, and two other anonymous reviewers for their constructive reviews and feedbacks. We would like to thank Dr. Pengfei Ma for the instructions in modelling. We also thank our Tibetan compatriots, Danzhen and Bazhu, who did a lot of favor in field work. We thank Dr. Zhiming Duan who provided information about boreholes in

1
2
3
4
5
6
7
8
9
10
11
12
13
14
15
16
17
18
19
20
21
22
23
24
25
26
27
28
29
30
31
32
33
34
35
36
37
38
39
40
41
42
43
44
45
46
47
48
49
50
51
52
53
54
55
56
57
58
59
60

Qiangtang. This research was financially supported by Ministry of Science and Technology of the People's Republic of China (2017YFC0601400-05), the China Geological Survey Project (DD20160027) and National Natural Science Foundation of China (41572188).

REFERENCES

ABADI, A.M., WEES, J.-D.V., DIJK, P.M.V. & CLOETINGH, S.A.P.L. (2005) Tectonics and Subsidence Evolution of the Sirt Basin, Libya. AAPG Bulletin, 92, 993-1027.

ABDULLAYEV, N.A., KADIROV, F. & GULIYEV, I.S. (2017) Subsidence History and Basin-Fill Evolution in the South Caspian Basin from Geophysical Mapping, Flexural Backstripping, Forward Lithospheric Modelling and Gravity Modelling. Geological Society, London, Special Publications, 427, 175-196.

ALLEN, P.A., ALLEN, J.R. (2005) Basin Analysis, Principles and Applications, second edn. Blackwell Publishing, Oxford, UK.

ARGAND, E. (1922). La Tectonique De L'asie. Congrès géologique international (XIIIe session), Belgique.

ARMSTRONG, P.A. (2005) Thermochronometers in Sedimentary Basins. Low-Temperature Thermochronology: Techniques, Interpretations, and Applications, 58, 499-525.

BAI, Y.S., LI, L., NIU, Z.J. & CUI, J.L. (2005) Characteristics and Tectonic Setting of Erlongba Formation Volcanic Rocks in Geladandong Area of Central

- 1
2
3
4 727 Qiangtang. *Acta Geoscientia Sinica*, 26, 113-120 (in Chinese with English
5
6 728 abstract).
- 7
8
9 729 BERNET, M., ZATTIN, M., GARVER, J.I., BRANDON, M.T. & VANCE, J.A.
10
11 730 (2001) Steady-State Exhumation of the European Alps. *Geology*, 29, 35-38.
- 12
13
14 731 BERTRAM, G.T. & MILTON, N.J. (1988) Reconstructing Basin Evolution from
15
16 732 Sedimentary Thickness; the Importance of Palaeobathymetric Control, with
17
18 733 Reference to the North Sea. *Basin Research*, 1, 247-257.
- 19
20
21 734 BLISNIUK, P.M., HACKER, B.R., GLODNY, J., RATSCHBACHER, L., BI, S.,
22
23 735 WU, Z., MCWILLIAMS, M.O. & CALVERT, A. (2001) Normal Faulting in
24
25 736 Central Tibet since at Least 13.5 Myr Ago. *Nature*, 412, 628.
- 26
27
28 737 BOND, G.C. & KOMINZ, M.A. (1984) Construction of Tectonic Subsidence Curves
29
30 738 for the Early Paleozoic Miogeocline, Southern Canadian Rocky Mountains:
31
32 739 Implications for Subsidence Mechanisms, Age of Breakup, and Crustal Thinning.
33
34 740 *Geol. Soc. Am. Bull.*, 95, 155-173.
- 35
36
37 741 BRUNET, M.F., KOROTAEV, M.V., ERSHOV, A.V. & NIKISHIN, A.M. (2003)
38
39 742 The South Caspian Basin: A Review of Its Evolution from Subsidence
40
41 743 Modelling. *Sedimentary Geology*, 156, 119-148.
- 42
43
44 744 BUSBY, C.J. & INGERSOLL, R.V. (1995) *Tectonics of Sedimentary Basins*.
45
46 745 Blackwell Science, Cambridge.
- 47
48
49 746 CARRAPA, B. & GARCIA-GASTELLANOS, D. (2005) Western Alpine
50
51 747 Back-Thrusting as Subsidence Mechanism in the Western Po Basin.
52
53 748 *Tectonophysics*, 406, 197-212.
- 54
55
56
57
58
59
60

1
2
3
4
5
6
7
8
9
10
11
12
13
14
15
16
17
18
19
20
21
22
23
24
25
26
27
28
29
30
31
32
33
34
35
36
37
38
39
40
41
42
43
44
45
46
47
48
49
50
51
52
53
54
55
56
57
58
59
60

749 CEDERBOM, C.E., SINCLAIR, H.D., SCHLUNEGGER, F. & RAHN, M.K. (2004)
750 Climate-Induced Rebound and Exhumation of the European Alps. *Geology*, 32,
751 709-712.

752 CHANG, E.Z. (2000) Geology and Tectonics of the Songpan-Ganzi Fold Belt,
753 Southwestern China. *Int Geol Rev*, 42, 813-831.

754 CHEN, J.L., WU, J.B., XU, J.F., DONG, Y.H., WANG, B.D. & KANG, Z.Q. (2013)
755 Geochemistry of Eocene High-Mg# Adakitic Rocks in the Northern Qiangtang
756 Terrane, Central Tibet: Implications for Early Uplift of the Plateau. *Geol. Soc.*
757 *Am. Bull.*, 125, 1800-1819.

758 CHEN, L., JENKYNS, H.C., XU, G., MATTIOLI, E., DA, X., YI, H., XIA, M., ZHU,
759 Z. & HUANG, Z. (2016) Preliminary Nannofossil and Geochemical Data from
760 Jurassic Black Shales from the Qiangtang Basin, Northern Tibet. *J. Asian Earth*
761 *Sci.*, 115, 257-267.

762 CHEN, L., XU, G.W., DA, X.J., JI, C.J. & YI, H.S. (2014) Biomarkers of Middle to
763 Late Jurassic Marine Sediments from a Canonical Section: New Records from
764 the Yanshiping Area, Northern Tibet. *Mar Petrol Geol*, 51, 256-267.

765 CHEN, S.S., FAN, W.M., SHI, R.D., GONG, X.H. & WU, K. (2017a) Removal of
766 Deep Lithosphere in Ancient Continental Collisional Orogens: A Case Study
767 from Central Tibet, China. *Geochemistry, Geophysics, Geosystems*, 18,
768 1225-1243.

769 CHEN, W., ZHANG, S., DING, J., ZHANG, J., ZHAO, X., ZHU, L., YANG, W.,
770 YANG, T., LI, H. & WU, H. (2017b) Combined Paleomagnetic and

- 771 Geochronological Study on Cretaceous Strata of the Qiangtang Terrane, Central
772 Tibet. *Gondwana Research*, 41, 373-389.
- 773 CHENG, L., WANG, J., WAN, Y., FU, X. & ZHONG, L. (2017) Astrochronology of
774 the Middle Jurassic Buqu Formation (Tibet, China) and Its Implications for the
775 Bathonian Time Scale. *Palaeogeography, Palaeoclimatology, Palaeoecology*,
776 487, 51-58.
- 777 CHRISTIE-BLICK, N. & BIDDLE, K.T. (1985) Deformation and Basin Formation
778 Along Strike-Slip Faults. In: *Strike-Slip Deformation, Basin Formation, and*
779 *Sedimentation* (Ed. by K. T. Biddle & N. Christie-Blick), 1-34. Society of
780 Economic Paleontologists and Mineralogists, Tulsa, OK, USA.
- 781 DAI, J., WANG, C., HÉBERT, R., LI, Y., ZHONG, H., GUILLAUME, R., BEZARD,
782 R. & WEI, Y. (2011) Late Devonian Oib Alkaline Gabbro in the Yarlung
783 Zangbo Suture Zone: Remnants of the Paleo-Tethys? *Gondwana Research*, 19,
784 232-243.
- 785 DAN, W., WANG, Q., WHITE, W.M., ZHANG, X.-Z., TANG, G.-J., JIANG, Z.-Q.,
786 HAO, L.-L. & OU, Q. (2018) Rapid Formation of Eclogites During a Nearly
787 Closed Ocean: Revisiting the Pianshishan Eclogite in Qiangtang, Central Tibetan
788 Plateau. *Chem. Geol.*, 477, 112-122.
- 789 DECELLES, P.G. & GILES, K.A. (1996) Foreland Basin Systems. *Basin research*, 8,
790 105-123.
- 791 DEWEY, J.F., SHACKLETON, R.M., CHENGFA, C. & YIYIN, S. (1988) The
792 Tectonic Evolution of the Tibetan Plateau. *Philosophical Transactions of the*

1
2
3
4
5
6
7
8
9
10
11
12
13
14
15
16
17
18
19
20
21
22
23
24
25
26
27
28
29
30
31
32
33
34
35
36
37
38
39
40
41
42
43
44
45
46
47
48
49
50
51
52
53
54
55
56
57
58
59
60

Royal Society of London A: Mathematical, Physical and Engineering Sciences,
327, 379-413.

DING, L., XU, Q., YUE, Y., WANG, H., CAI, F. & LI, S. (2014) The Andean-Type
Gangdese Mountains: Paleoelevation Record from the Paleocene–Eocene
Linzhou Basin. *Earth Planet. Sci. Lett.*, 392, 250-264.

DING, L., YANG, D., CAI, F.L., PULLEN, A., KAPP, P., GEHRELS, G.E., ZHANG,
L.Y., ZHANG, Q.H., LAI, Q.Z., YUE, Y.H. & SHI, R.D. (2013a) Provenance
Analysis of the Mesozoic Hoh-Xil-Songpan-Ganzi Turbidites in Northern Tibet:
Implications for the Tectonic Evolution of the Eastern Paleo-Tethys Ocean.
Tectonics, 32, 34-48.

DING, W.L., WAN, H., ZHANG, Y.Q. & HAN, G.Z. (2013b) Characteristics of the
Middle Jurassic Marine Source Rocks and Prediction of Favorable Source Rock
Kitchens in the Qiangtang Basin of Tibet. *J. Asian Earth Sci.*, 66, 63-72.

DONELICK, R.A., O'SULLIVAN, P.B. & KETCHAM, R.A. (2005) Apatite
Fission-Track Analysis. Low-Temperature Thermochronology: Techniques,
Interpretations, and Applications, 58, 49-94.

DRESSEL, I., SCHECK-WENDEROTH, M. & CACACE, M. (2017) Backward
Modelling of the Subsidence Evolution of the Colorado Basin, Offshore
Argentina and Its Relation to the Evolution of the Conjugate Orange Basin,
Offshore Sw Africa. *Tectonophysics*, 716, 168-181.

DUNKL, I. (2002) Trackkey: A Windows Program for Calculation and Graphical
Presentation of Fission Track Data. *Comput Geosci-Uk*, 28, 3-12.

- 1
2
3
4 815 EINSELE, G. (1992) Sedimentary Basins: Evolution, Facies, and Sediment Budget.
5
6 816 Springer-Verlag, Berlin.
7
8
9 817 FAN, J.J., LI, C., LIU, Y.M. & XU, J.X. (2015) Age and Nature of the Late Early
10
11 818 Cretaceous Zhaga Formation, Northern Tibet: Constraints on When the
12
13 819 Bangong-Nujiang Neo-Tethys Ocean Closed. *Int Geol Rev*, 57, 342-353.
14
15
16
17 820 FAN, J.J., LI, C., WU, H., ZHANG, T.Y., WANG, M., CHEN, J.W. & XU, J.X.
18
19 821 (2016) Late Jurassic Adakitic Granodiorite in the Dong Co Area, Northern Tibet:
20
21 822 Implications for Subduction of the Bangong–Nujiang Oceanic Lithosphere and
22
23 823 Related Accretion of the Southern Qiangtang Terrane. *Tectonophysics*, 691, Part
24
25 824 B, 345-361.
26
27
28
29
30 825 FANG, X., SONG, C., YAN, M., ZAN, J., LIU, C., SHA, J., ZHANG, W., ZENG, Y.,
31
32 826 WU, S. & ZHANG, D. (2016) Mesozoic Litho- and Magneto-Stratigraphic
33
34 827 Evidence from the Central Tibetan Plateau for Megamonsoon Evolution and
35
36 828 Potential Evaporites. *Gondwana Research*, 37, 110-129.
37
38
39
40 829 FU, X.G., WANG, J., TAN, F.W., CHEN, M. & CHEN, W.B. (2010) The Late
41
42 830 Triassic Rift-Related Volcanic Rocks from Eastern Qiangtang, Northern Tibet
43
44 831 (China): Age and Tectonic Implications. *Gondwana Research*, 17, 135-144.
45
46
47
48 832 FU, X.G., WANG, J., WANG, Z.J. & CHEN, W.X. (2007) Identification of
49
50 833 Sedimentary Gap between the Late Triassic Nadi Kangri Formation and Its
51
52 834 Underlying Strata in the Qiangtang Basin, Northern Tibet and Its Geological
53
54 835 Significance. *Geological Review*, 53, 329-336 (in Chinese with English abstract).
55
56
57
58 836 GALBRAITH, R. (1981) On Statistical Models for Fission Track Counts.
59
60

1
2
3
4
5
6
7
8
9
10
11
12
13
14
15
16
17
18
19
20
21
22
23
24
25
26
27
28
29
30
31
32
33
34
35
36
37
38
39
40
41
42
43
44
45
46
47
48
49
50
51
52
53
54
55
56
57
58
59
60

837 Mathematical Geology, 13, 471-478.

838 GALBRAITH, R.F. (2005) Statistics for Fission Track Analysis. CRC Press.

839 GALBRAITH, R.F. & GREEN, P.F. (1990) Estimating the Component Ages in a

840 Finite Mixture. Nucl Tracks Rad Meas, 17, 197-206.

841 GLEADOW, A. (1981) Fission-Track Dating Methods: What Are the Real

842 Alternatives? Nuclear Tracks, 5, 3-14.

843 GREEN, P. (1981) A New Look at Statistics in Fission-Track Dating. Nuclear tracks,

844 5, 77-86.

845 GRADSTEIN, F.M., OGG, J.G., SMITH, A.G., BLEEKER, W. & LOURENS, L.J.

846 (2004) A New Geologic Time Scale, with Special Reference to Precambrian and

847 Neogene. *Episodes*, 27, 83-100.

848 GUYNN, J.H., KAPP, P., PULLEN, A., HEIZLER, M., GEHRELS, G. & DING, L.

849 (2006) Tibetan Basement Rocks near Amdo Reveal “Missing” Mesozoic

850 Tectonism Along the Bangong Suture, Central Tibet. *Geology*, 34, 505-508.

851 HE, J.L., WANG, J., TAN, F.W., CHEN, M., LI, Z.X., SUN, T., WANG, P.K., DU,

852 B.W. & CHEN, W.B. (2014) A Comparative Study between Present and

853 Palaeo-Heat Flow in the Qiangtang Basin, Northern Tibet, China. Marine and

854 Petroleum Geology, 57, 345-358.

855 HOLT, P.J., ALLEN, M.B. & VAN HUNEN, J. (2015) Basin Formation by Thermal

856 Subsidence of Accretionary Orogens. *Tectonophysics*, 639, 132-143.

857 HOLT, P.J., ALLEN, M.B., VAN HUNEN, J. & BJØRNSETH, H.M. (2010)

858 Lithospheric Cooling and Thickening as a Basin Forming Mechanism.

- 859 *Tectonophysics*, 495, 184-194.
- 860 HOMEWOOD, P., ALLEN, P.A. & WILLIAMS, G.D. (1986) Dynamics of the
 861 Molasse Basin of Western Switzerland. In: Foreland Basins (Ed. by P. A. Allen
 862 & P. Homewood), 199-217. Special Publication of the International Association
 863 of Sedimentologists, Blackwell Science, Oxford.
- 864 HORTON, B.K. (2012) Cenozoic Evolution of Hinterland Basins in the Andes and
 865 Tibet. In: *Tectonics of Sedimentary Basins: Recent Advances* (Ed. by C. Busby
 866 & A. Azor), 427-444. John Wiley & Sons, Ltd.
- 867 HORTON, B.K. (2018) Sedimentary Record of Andean Mountain Building.
 868 *Earth-Science Reviews*, 178, 279-309.
- 869 HUANG, Q.T., LIU, W.L., XIA, B., CAI, Z.R., CHEN, W.Y., LI, J.F. & YIN, Z.X.
 870 (2017) Petrogenesis of the Majiari Ophiolite (Western Tibet, China):
 871 Implications for Intra-Oceanic Subduction in the Bangong–Nujiang Tethys. *J.*
 872 *Asian Earth Sci.*, 146, 337-351.
- 873 HURFORD, A.J. & GREEN, P.F. (1983) The Zeta-Age Calibration of Fission-Track
 874 Dating. *Isot Geosci*, 1, 285-317.
- 875 JORDAN, T.E. (1981) Thrust Loads and Foreland Basin Evolution, Cretaceous,
 876 Western United States. *AAPG bulletin*, 65, 2506-2520.
- 877 KAPP, P., DECELLES, P.G., GEHRELS, G.E., HEIZLER, M. & DING, L. (2007)
 878 Geological Records of the Lhasa-Qiangtang and Indo-Asian Collisions in the
 879 Nima Area of Central Tibet. *Geol. Soc. Am. Bull.*, 119, 917-933.
- 880 KAPP, P., YIN, A., HARRISON, T.M. & DING, L. (2005) Cretaceous-Tertiary

1
2
3
4
5
6
7
8
9
10
11
12
13
14
15
16
17
18
19
20
21
22
23
24
25
26
27
28
29
30
31
32
33
34
35
36
37
38
39
40
41
42
43
44
45
46
47
48
49
50
51
52
53
54
55
56
57
58
59
60

881 Shortening, Basin Development, and Volcanism in Central Tibet. *Geol. Soc. Am.*
882 *Bull.*, 117, 865-878.

883 KAPP, P., YIN, A., MANNING, C.E., HARRISON, T.M., TAYLOR, M.H. & DING,
884 L. (2003) Tectonic Evolution of the Early Mesozoic Blueschist-Bearing
885 Qiangtang Metamorphic Belt, Central Tibet. *Tectonics*, 22.

886 KAPP, P., YIN, A., MANNING, C.E., MURPHY, M., HARRISON, T.M., SPURLIN,
887 M., LIN, D., DENG, X.G. & WU, C.M. (2000) Blueschist-Bearing Metamorphic
888 Core Complexes in the Qiangtang Block Reveal Deep Crustal Structure of
889 Northern Tibet. *Geology*, 28, 19-22.

890 KETCHAM, R.A. (2005) The Role of Crystallographic Angle in Characterizing and
891 Modeling Apatite Fission-Track Length Data. *Radiation Measurements*, 39,
892 595-601.

893 KETCHAM, R.A., CARTER, A., DONELICK, R.A., BARBARAND, J. &
894 HURFORD, A.J. (2007) Improved Modeling of Fission-Track Annealing in
895 Apatite. *American Mineralogist*. 92, 799-810.

896 KETCHAM, R.A., DONELICK, R.A. & CARLSON, W.D. (1999) Variability of
897 Apatite Fission-Track Annealing Kinetics: Iii. Extrapolation to Geological Time
898 Scales. *Am Mineral*, 84, 1235-1255.

899 KNELLER, B.C. (1991) A Foreland Basin on the Southern Margin of Iapetus.
900 *Journal of the Geological Society*, 148, 207-210.

901 KUHN, P.P., ECHTLER, H., LITTKE, R. & ALFARO, G. (2010) Thermal Basin
902 Modelling of the Arauco Forearc Basin, South Central Chile—Heat Flow and

- 903 Active Margin Tectonics. *Tectonophysics*, 495, 111-128.
- 904 LI, C., CHENG, L., HU, K., YANG, Z. & HONG, Y. (1995) Study on the
905 Paleo-Tethys Suture Zone of Lungmu Co-Shuanghu, Tibet. Geological
906 Publishing House, Beijing.
- 907 LI, G.M., LI, J.X., ZHAO, J.X., QIN, K.Z., CAO, M.J. & EVANS, N.J. (2015a)
908 Petrogenesis and Tectonic Setting of Triassic Granitoids in the Qiangtang
909 Terrane, Central Tibet: Evidence from U-Pb Ages, Petrochemistry and Sr-Nd-Hf
910 Isotopes. *J. Asian Earth Sci.*, 105, 443-455.
- 911 LI, G.M., QIN, K.Z., LI, J.X., EVANS, N.J., ZHAO, J.X., CAO, M.J. & ZHANG,
912 X.N. (2017a) Cretaceous Magmatism and Metallogeny in the Bangong–Nujiang
913 Metallogenic Belt, Central Tibet: Evidence from Petrogeochemistry, Zircon
914 U–Pb Ages, and Hf–O Isotopic Compositions. *Gondwana Research*, 41,
915 110-127.
- 916 LI, H.Q., XU, Z.Q., WEBB, A.A.G., LI, T.F., MA, S.W. & HUANG, X.M. (2017c)
917 Early Jurassic Tectonism Occurred within the Basu Metamorphic Complex,
918 Eastern Central Tibet: Implications for an Archipelago-Acretion Orogenic
919 Model. *Tectonophysics*, 702, 29-41.
- 920 LI, J. & BATTEN, D.J. (2004) Early Cretaceous Palynofloras from the Tanggula
921 Mountains of the Northern Qinghai-Xizang (Tibet) Plateau, China. *Cretaceous*
922 *Research*, 25, 531-542.
- 923 LI, S., DING, L., GUILMETTE, C., FU, J., XU, Q., YUE, Y. & HENRIQUE-PINTO,
924 R. (2017b) The Subduction-Acretion History of the Bangong-Nujiang Ocean:

1
2
3
4
5
6
7
8
9
10
11
12
13
14
15
16
17
18
19
20
21
22
23
24
25
26
27
28
29
30
31
32
33
34
35
36
37
38
39
40
41
42
43
44
45
46
47
48
49
50
51
52
53
54
55
56
57
58
59
60

925 Constraints from Provenance and Geochronology of the Mesozoic Strata near
926 Gaize, Central Tibet. *Tectonophysics*, 702, 42-60.

927 LI, Y., HE, J., HAN, Z., WANG, C., MA, P., ZHOU, A., LIU, S.-A. & XU, M. (2016)
928 Late Jurassic Sodium-Rich Adakitic Intrusive Rocks in the Southern Qiangtang
929 Terrane, Central Tibet, and Their Implications for the Bangong–Nujiang Ocean
930 Subduction. *Lithos*, 245, 34-46.

931 LI, Y., HE, J., WANG, C., HAN, Z., MA, P., XU, M. & DU, K. (2015c) Cretaceous
932 Volcanic Rocks in South Qiangtang Terrane: Products of Northward Subduction
933 of the Bangong–Nujiang Ocean? *J. Asian Earth Sci.*, 104, 69-83.

934 LI, Y., HE, J., WANG, C., SANTOSH, M., DAI, J., ZHANG, Y., WEI, Y. & WANG,
935 J. (2013) Late Cretaceous K-Rich Magmatism in Central Tibet: Evidence for
936 Early Elevation of the Tibetan Plateau? *Lithos*, 160, 1-13.

937 LI, Y., WANG, C., DAI, J., XU, G., HOU, Y. & LI, X. (2015b) Propagation of the
938 Deformation and Growth of the Tibetan–Himalayan Orogen: A Review.
939 *Earth-Science Reviews*, 143, 36-61.

940 LI, Y., WANG, C. & YI, H. (2002) Filled Sequence and Evolution of the Mesozoic
941 Qiangtang Composite Foreland Basin in the Qinghai-Tibet Plateau. *Journal of*
942 *Stratigraphy*, 26, 62-67 (in Chinese with English abstract).

943 LI, Y., WANG, C. & YI, H. (2003) The Late Triassic Collision and Sedimentary
944 Responses at Western Segment of Jinshajing Suture, Tibet. *Acta sedimentologica*
945 *sinica*, 21, 191-197 (in Chinese with English abstract).

946 LI, Y., WANG, C., YI, H., SHI, H., LIN, J., ZHU, L. & LI, X. (2001) Fill Models of

- in the Qiangtang Composite Foreland Basin in Qinghai-Xizang Plateau, China.
- Acta Sedimentologica Sinica*, 19, 20-27 (in Chinese with English abstract).
- LIANG, X., WANG, G., YANG, B., RAN, H., ZHENG, Y., DU, J. & LI, L. (2017)
- Stepwise Exhumation of the Triassic Lanling High-Pressure Metamorphic Belt in
- Central Qiangtang, Tibet: Insights from a Coupled Study of Metamorphism,
- Deformation and Geochronology. *Tectonics*, 36, 652-670.
- LIU, D., SHI, R., DING, L., HUANG, Q., ZHANG, X., YUE, Y. & ZHANG, L.
- (2017) Zircon U–Pb Age and Hf Isotopic Compositions of Mesozoic Granitoids
- in Southern Qiangtang, Tibet: Implications for the Subduction of the
- Bangong–Nujiang Tethyan Ocean. *Gondwana Research*, 41, 157-172.
- LIU, Y., SANTOSH, M., ZHAO, Z.B., NIU, W.C. & WANG, G.H. (2011) Evidence
- for Palaeo-Tethyan Oceanic Subduction within Central Qiangtang, Northern
- Tibet. *Lithos*, 127, 39-53.
- LU, L., ZHANG, K. J., YAN, L. L., JIN, X. & ZHANG, Y. X. (2017) Was Late
- Triassic Tanggula Granitoid (Central Tibet, Western China) a Product of Melting
- of Underthrust Songpan-Ganzi Flysch Sediments? *Tectonics*, 36, 902-928.
- MAGOON, L.B. & DOW, W.G. (1994) The Petroleum System. In: The Petroleum
- System: From Source to Trap (Ed. by L. B. Magoon & W. G. Dow), 60, 3-24.
- American Association of Petroleum Geologists Memoir.
- MIALL, A. (1995) Collision-Related Foreland Basins. In: Tectonics of Sedimentary
- Basins (Ed. by C. J. Busby & R. V. Ingersoll), 393-424. Blackwell Science,
- Oxford, UK.

1
2
3
4
5
6
7
8
9
10
11
12
13
14
15
16
17
18
19
20
21
22
23
24
25
26
27
28
29
30
31
32
33
34
35
36
37
38
39
40
41
42
43
44
45
46
47
48
49
50
51
52
53
54
55
56
57
58
59
60

969 MILLER, K.G., KOMINZ, M.A., BROWNING, J.V., WRIGHT, J.D., MOUNTAIN,
970 G.S., KATZ, M.E., SUGARMAN, P.J., CRAMER, B.S., CHRISTIE-BLICK, N.
971 & PEKAR, S.F. (2005) The Phanerozoic Record of Global Sea-Level Change.
972 *Science*, 310, 1293-1298.

973 MITROVICA, J.X., BEAUMONT, C. & JARVIS, G.T. (1989) Tilting of Continental
974 Interiors by the Dynamical Effects of Subduction. *Tectonics*, 8, 1079-1094.

975 MURPHY, M.A., YIN, A., HARRISON, T.M., DÜRR, S.B., CHEN, Z., RYERSON,
976 F.J., KIDD, W.S.F., WANG, X. & ZHOU, X. (1997) Did the Indo-Asian
977 Collision Alone Create the Tibetan Plateau? *Geology*, 25, 719-722.

978 NAESER, N.D., NAESER, C.W. & MCCULLOH, T.H. (1989) The Application of
979 Fission-Track Dating to the Depositional and Thermal History of Rocks in
980 Sedimentary Basins. In: Thermal History of Sedimentary Basins (Ed. by N.
981 Naeser & T. McCulloh), 157-180. Springer.

982 NAYLOR, M. & SINCLAIR, H.D. (2008) Pro- Vs. Retro-Foreland Basins. *Basin*
983 *Research*, 20, 285-303.

984 NIE, S., YIN, A., ROWLEY, D.B. & JIN, Y. (1994) Exhumation of the Dabie Shan
985 Ultra-High-Pressure Rocks and Accumulation of the Songpan-Ganzi Flysch
986 Sequence, Central China. *Geology*, 22, 999-1002.

987 OGG, J.G., OGG, G. & GRADSTEIN, F.M. (2008) The Concise Geologic Time
988 Scale. Cambridge University Press.

989 O’SULLIVAN, P.B. & PARRISH, R.R. (1995) The Importance of Apatite
990 Composition and Single-Grain Ages When Interpreting Fission-Track Data from

- 1
- 2
- 3
- 4 991 Plutonic Rocks-a Case-Study from the Coast Ranges, British-Columbia. Earth
- 5
- 6 992 Planet. Sci. Lett., 132, 213-224.
- 7
- 8
- 9 993 OU, Q., WANG, Q., WYMAN, D.A., ZHANG, H.X., YANG, J.H., ZENG, J.P.,
- 10
- 11 994 HAO, L.L., CHEN, Y.W., LIANG, H. & QI, Y. (2017) Eocene Adakitic
- 12
- 13 995 Porphyries in the Central - Northern Qiangtang Block, Central Tibet: Partial
- 14
- 15 996 Melting of Thickened Lower Crust and Implications for Initial Surface Uplifting
- 16
- 17 997 of the Plateau. *Journal of Geophysical Research: Solid Earth*, 122, 1025-1053.
- 18
- 19 998 PEARCE, J.A. & HOUJUN, M. (1988) Volcanic Rocks of the 1985 Tibet Geotraverse:
- 20
- 21 999 Lhasa to Golmud. *Philosophical Transactions of the Royal Society of London A:*
- 22
- 23 1000 *Mathematical, Physical and Engineering Sciences*, 327, 169-201.
- 24
- 25 1001 PERSANO, C., STUART, F.M., BISHOP, P. & DEMPSTER, T.J. (2005)
- 26
- 27 1002 Deciphering Continental Breakup in Eastern Australia Using Low-Temperature
- 28
- 29 1003 Thermochronometers. *Journal of Geophysical Research: Solid Earth*, 110.
- 30
- 31 1004 PULLEN, A. & KAPP, P. (2014) Mesozoic Tectonic History and Lithospheric
- 32
- 33 1005 Structure of the Qiangtang Terrane: Insights from the Qiangtang Metamorphic
- 34
- 35 1006 Belt, Central Tibet. *Geological Society of America Special Papers*, 507.
- 36
- 37 1007 PULLEN, A., KAPP, P., GEHRELS, G.E., VERVOORT, J.D. & DING, L. (2008)
- 38
- 39 1008 Triassic Continental Subduction in Central Tibet and Mediterranean-Style
- 40
- 41 1009 Closure of the Paleo-Tethys Ocean. *Geology*, 36, 351-354.
- 42
- 43 1010 REINERS, P.W. & BRANDON, M.T. (2006) Using Thermochronology to
- 44
- 45 1011 Understand Orogenic Erosion. *Annu. Rev. Earth Planet. Sci.*, 34, 419-466.
- 46
- 47 1012 REN, Z.L., CUI, J.P., LIU, C.Y., LI, T.J., CHEN, G., DOU, S., TIAN, T. & LUO,
- 48
- 49
- 50
- 51
- 52
- 53
- 54
- 55
- 56
- 57
- 58
- 59
- 60

1
2
3
4
5
6
7
8
9
10
11
12
13
14
15
16
17
18
19
20
21
22
23
24
25
26
27
28
29
30
31
32
33
34
35
36
37
38
39
40
41
42
43
44
45
46
47
48
49
50
51
52
53
54
55
56
57
58
59
60

1013 Y.T. (2015) Apatite Fission Track Evidence of Uplift Cooling in the Qiangtang
1014 Basin and Constraints on the Tibetan Plateau Uplift. *Acta Geol Sin-Engl*, 89,
1015 467-484.

1016 ROGER, F., JOLIVET, M., CATTIN, R. & MALAVIEILLE, J. (2011)
1017 Mesozoic-Cenozoic Tectonothermal Evolution of the Eastern Part of the Tibetan
1018 Plateau (Songpan-Garzê, Longmen Shan Area): Insights from
1019 Thermochronological Data and Simple Thermal Modelling. Geological Society,
1020 London, Special Publications, 353, 9-25.

1021 ROHRMANN, A., KAPP, P., CARRAPA, B., REINERS, P.W., GUYNN, J., DING,
1022 L. & HEIZLER, M. (2012) Thermochronologic Evidence for Plateau Formation
1023 in Central Tibet by 45 Ma. *Geology*, 40, 187-190.

1024 ROWLEY, D.B. & CURRIE, B.S. (2006) Palaeo-Altometry of the Late Eocene to
1025 Miocene Lunpola Basin, Central Tibet. *Nature*, 439, 677-681.

1026 ROYDEN, L. & KEEN, C.E. (1980) Rifting Process and Thermal Evolution of the
1027 Continental Margin of Eastern Canada Determined from Subsidence Curves.
1028 *Earth Planet. Sci. Lett.*, 51, 343-361.

1029 SACHSENHOFER, R.F., LANKREIJER, A., CLOETINGH, S. & EBNER, F. (1997)
1030 Subsidence Analysis and Quantitative Basin Modelling in the Styrian Basin
1031 (Pannonian Basin System, Austria). *Tectonophysics*, 272, 175-196.

1032 SCIUNNACH, D. & GARZANTI, E. (2012) Subsidence History of the Tethys
1033 Himalaya. *Earth-Science Reviews*, 111, 179-198.

1034 SCLATER, J.G. & CHRISTIE, P.A.F. (1980) Continental Stretching: An Explanation

- 1035 of the Post-Mid-Cretaceous Subsidence of the Central North Sea Basin. *Journal*
1036 *of Geophysical Research: Solid Earth*, 85, 3711-3739.
- 1037 SILVIA, O.S., RAMON, S., JOAN, G., ROBERT, O., RAMON, M., JOS é , A.,
1038 ISABEL, S.R. & LUIS, M. (2017) Subsidence and Thermal History of an
1039 Inverted Late Jurassic-Early Cretaceous Extensional Basin (Cameros,
1040 North-Central Spain) Affected by Very Low- to Low-Grade Metamorphism.
1041 *Basin Research*, 29, 156-174.
- 1042 SINCLAIR, H.D. & NAYLOR, M. (2012) Foreland Basin Subsidence Driven by
1043 Topographic Growth Versus Plate Subduction. *Geol. Soc. Am. Bull.*, 124,
1044 368-379.
- 1045 SOBEL, E.R. & SEWARD, D. (2010) Influence of Etching Conditions on Apatite
1046 Fission-Track Etch Pit Diameter. *Chem. Geol.*, 271, 59-69.
- 1047 SONG, C., ZENG, Y., YAN, M., FANG, X., FENG, Y., PAN, J., LIU, X., MENG, Q.,
1048 HU, C. & ZHONG, S. (2017) Sedimentary Conditions of Evaporites in the Late
1049 Jurassic Xiali Formation, Qiangtang Basin: Evidence from Geochemistry
1050 Records. *Acta Geologica Sinica - English Edition*, 91, 156-174.
- 1051 SONG, C.Y. (2012) Evolution of Mesozoic Sedimentary Basin in Qiangtang and Its
1052 Significance in Petroleum Geology, Chinese Academy of Geological Sciences,
1053 Beijing (in Chinese with English abstract).
- 1054 SONG, P., DING, L., LI, Z., LIPPERT, P.C. & YUE, Y. (2017) An Early Bird from
1055 Gondwana: Paleomagnetism of Lower Permian Lavas from Northern Qiangtang
1056 (Tibet) and the Geography of the Paleo-Tethys. *Earth and Planetary Science*

1
2
3
4
5
6
7
8
9
10
11
12
13
14
15
16
17
18
19
20
21
22
23
24
25
26
27
28
29
30
31
32
33
34
35
36
37
38
39
40
41
42
43
44
45
46
47
48
49
50
51
52
53
54
55
56
57
58
59
60

1057 Letters, 475, 119-133.

1058 STAPEL, G., CLOETINGH, S. & PRONK, B. (1996) Quantitative Subsidence
1059 Analysis of the Mesozoic Evolution of the Lusitanian Basin (Western Iberian
1060 Margin). *Tectonophysics*, 266, 493-507.

1061 STECKLER, M.S. & WATTS, A.B. (1978) Subsidence of the Atlantic-Type
1062 Continental Margin Off New York. *Earth Planet. Sci. Lett.*, 41, 1-13.

1063 TANG, M., LIU-ZENG, J., HOKE, G.D., XU, Q., WANG, W., LI, Z., ZHANG, J. &
1064 WANG, W. (2017) Paleoelevation Reconstruction of the Paleocene-Eocene
1065 Gonjo Basin, Se-Central Tibet. *Tectonophysics*, 712–713, 170-181.

1066 TIAN, Y., KOHN, B.P., HU, S. & GLEADOW, A.J.W. (2014) Postorogenic Rigid
1067 Behavior of the Eastern Songpan-Ganze Terrane: Insights from
1068 Low-Temperature Thermochronology and Implications for Intracontinental
1069 Deformation in Central Asia. *Geochemistry, Geophysics, Geosystems*, 15,
1070 453-474.

1071 TOZER, B., WATTS, A.B. & DALY, M.C. (2017) Crustal Structure, Gravity
1072 Anomalies, and Subsidence History of the Parnaíba Cratonic Basin, Northeast
1073 Brazil. *Journal of Geophysical Research: Solid Earth*, 122, 5591-5621.

1074 U.S. GEOLOGICAL SURVEY (2006) FGDC Digital Cartographic Standard for
1075 Geologic Map Symbolization (Postscript Implementation). U.S. Geological
1076 Survey Techniques and Methods 11-A2. <http://pubs.usgs.gov/tm/2006/11A02/>

1077 VERGÉS, J., MARZO, M., SANTAEULÀRIA, T., SERRA-KIEL, J., BURBANK,
1078 D.W., MUÑOZ, J.A. & GIMÉNEZ-MONTSANT, J. (1998) Quantified Vertical

- 1079 Motions and Tectonic Evolution of the Se Pyrenean Foreland Basin. In:
- 1080 Cenozoic Foreland Basins of Western Europe (Ed. by A. Mascle, C.
- 1081 Puigdefàbregas, H. P. Luterbacher & M. Fernàndez), 134, 107-134. Special
- 1082 Publications, Geological Society of London.
- 1083 VERMEESCH, P. (2012) On the Visualisation of Detrital Age Distributions. *Chem.*
- 1084 *Geol.*, 312-313, 190-194.
- 1085 WANG, C., DAI, J., ZHAO, X., LI, Y., GRAHAM, S.A., HE, D., RAN, B. & MENG,
- 1086 J. (2014) Outward-Growth of the Tibetan Plateau During the Cenozoic: A
- 1087 Review. *Tectonophysics*, 621, 1-43.
- 1088 WANG, C., YIN, H., LI, Y., DENG, B., LIU, D., WANG, G., SHI, H., LI, Y., MA, R.
- 1089 & LIN, J. (2001) The Geological Evolution and Prospective Oil and Gas
- 1090 Assessment of the Qiangtang Basin in Northern Tibetan Plateau. Geological
- 1091 Publishing House, Beijing.
- 1092 WANG, C.S., ZHAO, X.X., LIU, Z.F., LIPPERT, P.C., GRAHAM, S.A., COE, R.S.,
- 1093 YI, H.S., ZHU, L.D., LIU, S. & LI, Y.L. (2008b) Constraints on the Early Uplift
- 1094 History of the Tibetan Plateau. *Proc. Natl. Acad. Sci. U. S. A.*, 105, 4987-4992.
- 1095 WANG, J., FU, X., CHEN, W. & WANG, Z. (2007) The Late Triassic
- 1096 Paleo-Weathering Crust in the Qiangtang Basin, Northern Tibet: Geology,
- 1097 Geochemistry and Significance. *Acta Sedimentologica Sinica*, 25, 487 (in
- 1098 Chinese with English abstract).
- 1099 WANG, J., FU, X.G., CHEN, W.X., WANG, Z.J., TAN, F.W., CHEN, M. & ZHUO,
- 1100 J.W. (2008a) Chronology and Geochemistry of the Volcanic Rocks in Woruo

1
2
3
4
5
6
7
8
9
10
11
12
13
14
15
16
17
18
19
20
21
22
23
24
25
26
27
28
29
30
31
32
33
34
35
36
37
38
39
40
41
42
43
44
45
46
47
48
49
50
51
52
53
54
55
56
57
58
59
60

1101 Mountain Region, Northern Qiangtang Depression: Implications to the Late
1102 Triassic Volcanic-Sedimentary Events. *Sci. China Ser. D-Earth Sci.*, 51,
1103 194-205.

1104 WANG, J., TAN, F., LI, Y., LI, Y., CHEN, M., WANG, C., GUO, Z., WANG, X.,
1105 DU, B. & ZHU, Z. (2004b) The Potential of the Oil and Gas Resources in Major
1106 Sedimentary Basins on the Qinghai-Xizang Plateau. Geological Publishing
1107 House, Beijing.

1108 WANG, J., TAN, F., WANG, X., DU, B. & CHEN, M. (2004a) The Sedimentary and
1109 Tectonic Characteristics of Qiangtang Basin in the Early Jurassic in Northern
1110 Xizang (Tibet). *Acta Sedimentologica Sinica*, 22, 198-205 (in Chinese with
1111 English abstract).

1112 WANG, L.B., ZHANG, Y.Q., CAI, J.J. & HAN, G.Z. (2013) Characteristics of the
1113 Upper Jurassic Marine Source Rocks and Prediction of Favorable Source Rock
1114 Kitchens in the Qiangtang Basin, Tibet. *J Earth Sci-China*, 24, 815-829.

1115 WANG, L.C. & WEI, Y.S. (2013) Apatite Fission Track Thermochronology Evidence
1116 for the Mid-Cretaceous Tectonic Event in the Qiangtang Basin, Tibet. *Acta*
1117 *Petrologica Sinica*, 29, 1039-1047 (in Chinese with English abstract).

1118 WANG, Q., WYMAN, D.A., LI, Z.X., SUN, W., CHUNG, S.L., VASCONCELOS,
1119 P.M., ZHANG, Q., DONG, H., YU, Y. & PEARSON, N. (2010) Eocene
1120 North–South Trending Dikes in Central Tibet: New Constraints on the Timing of
1121 East–West Extension with Implications for Early Plateau Uplift? *Earth Planet.*
1122 *Sci. Lett.*, 298, 205-216.

- 1
2
3
4 1123 WANG, Z., WANG, J., FU, X., FENG, X., WANG, D., SONG, C., CHEN, W.,
5
6 1124 ZENG, S. & YU, F. (2017b) Provenance and Tectonic Setting of the Quemoco
7
8
9 1125 Sandstones in the North Qiangtang Basin, North Tibet: Evidence from
10
11 1126 Geochemistry and Detrital Zircon Geochronology. *Geological Journal*,
12
13
14 1127 <https://doi.org/10.1002/gj.2967>.
15
16
17 1128 WANG, Z., WANG, J., FU, X., ZHAN, W., YU, F., FENG, X., SONG, C., CHEN, W.
18
19 1129 & ZENG, S. (2017a) Organic Material Accumulation of Carnian Mudstones in
20
21 1130 the North Qiangtang Depression, Eastern Tethys: Controlled by the Paleoclimate,
22
23 1131 Paleoenvironment, and Provenance. *Mar Petrol Geol*, 88, 440-457.
24
25
26
27 1132 WATTS, A.B. & RYAN, W.B.F. (1976) Flexure of the Lithosphere and Continental
28
29 1133 Margin Basins. *Tectonophysics*, 36, 25-44.
30
31
32 1134 WATTS, A.B., KARNER, G.D. & STECKLER, M.S. (1982) Lithospheric Flexure
33
34 1135 and the Evolution of Sedimentary Basins. *Philosophical Transactions of the*
35
36 1136 *Royal Society of London A: Mathematical, Physical and Engineering Sciences*,
37
38 1137 305, 249-281.
39
40
41
42 1138 WEISLOGEL, A.L., GRAHAM, S.A., CHANG, E.Z., WOODEN, J.L., GEHRELS,
43
44 1139 G.E. & YANG, H. (2006) Detrital Zircon Provenance of the Late Triassic
45
46 1140 Songpan-Ganzi Complex: Sedimentary Record of Collision of the North and
47
48 1141 South China Blocks. *Geology*, 34, 97-100.
49
50
51
52 1142 WU, Z., WU, X., ZHAO, Z., LU, L., YE, P. & ZHANG, Y. (2014) Shrimp U–Pb
53
54 1143 Isotopic Dating of the Late Cretaceous Volcanic Rocks and Its Chronological
55
56 1144 Constraint on the Red-Beds in Southern Qiangtang Block. *Acta Geoscientica*
57
58
59
60

1
2
3
4
5
6
7
8
9
10
11
12
13
14
15
16
17
18
19
20
21
22
23
24
25
26
27
28
29
30
31
32
33
34
35
36
37
38
39
40
41
42
43
44
45
46
47
48
49
50
51
52
53
54
55
56
57
58
59
60

1145 *Sinica*, 35, 567-572 (in Chinese with English abstract).

1146 XU, Q., DING, L., ZHANG, L.Y., CAI, F.L., LAI, Q.Z., YANG, D. & JING, L.Z.

1147 (2013) Paleogene High Elevations in the Qiangtang Terrane, Central Tibetan

1148 Plateau. *Earth Planet. Sci. Lett.*, 362, 31-42.

1149 YAO, X., LIU, S., BAI, Y. & JI, H. (2017) Neogene Residual Subsidence and Its

1150 Response to a Sinking Slab in the Deep Mantle of Eastern China. *J. Asian Earth*

1151 *Sci.*, 143, 269-282.

1152 YAN, M., ZHANG, D., FANG, X., REN, H., ZHANG, W., ZAN, J., SONG, C. &

1153 ZHANG, T. (2016) Paleomagnetic Data Bearing on the Mesozoic Deformation

1154 of the Qiangtang Block: Implications for the Evolution of the Paleo-and

1155 Meso-Tethys. *Gondwana Research*, 39, 25.

1156 YANG, R., CAO, J., HU, G., BIAN, L., HU, K. & FU, X. (2017) Marine to Brackish

1157 Depositional Environments of the Jurassic–Cretaceous Suowa Formation,

1158 Qiangtang Basin (Tibet), China. *Palaeogeography, Palaeoclimatology,*

1159 *Palaeoecology*, 473, 41-56.

1160 YIN, A. & HARRISON, T.M. (2000) Geologic Evolution of the Himalayan-Tibetan

1161 Orogen. *Annu. Rev. Earth Planet. Sci.*, 28, 211-280.

1162 YIN, J. (2016) Bathonian–Callovian (Middle Jurassic) Ammonites from Northwestern

1163 Qiangtang Block, Tibet, and the Revised Age of the Suowa Formation.

1164 *Proceedings of the Geologists’ Association*, 127, 245-263.

1165 YIN, J. & CHANDLER, R.B. (2016) Aalenian to Lower Bajocian Ammonites from

1166 the Qiangtang Block (North Tibet). *Proceedings of the Geologists’ Association*,

- 1167 127, 170-186.
- 1168 ZENG, S., HU, X., LI, J., XU, S., FANG, H. & CAI, J. (2015) Detection of the Deep
 1169 Crustal Structure of the Qiangtang Terrane Using Magnetotelluric Imaging.
 1170 *Tectonophysics*, 661, 180-189.
- 1171 ZHAI, Q. & LI, C. (2007) Zircon Shrimp Dating of Volcanic Rock from Nadigangri
 1172 Formation in Juhuashan, Qiangtang, Northern Tibet and Its Geological
 1173 Significance. *Acta Geologica Sinica*, 81, 795-800 (in Chinese with English
 1174 abstract).
- 1175 ZHAI, Q.G., JAHN, B.M., SU, L., WANG, J., MO, X.X., LEE, H.Y., WANG, K.L.
 1176 & TANG, S.H. (2013) Triassic Arc Magmatism in the Qiangtang Area, Northern
 1177 Tibet: Zircon U-Pb Ages, Geochemical and Sr-Nd-Hf Isotopic Characteristics,
 1178 and Tectonic Implications. *J. Asian Earth Sci.*, 63, 162-178.
- 1179 ZHAI, Q.G., JAHN, B.M., WANG, J., HU, P.Y., CHUANG, S.L., LEE, H.Y., TANG,
 1180 S.H. & TANG, Y. (2015) Oldest Paleo-Tethyan Ophiolitic Mélange in the
 1181 Tibetan Plateau. *GSA Bulletin*, 128, 355-373.
- 1182 ZHANG, K.J. (2000) Cretaceous Palaeogeography of Tibet and Adjacent Areas
 1183 (China): Tectonic Implications. *Cretaceous Research*, 21, 23-33.
- 1184 ZHANG, K.J. & TANG, X.C. (2009) Eclogites in the Interior of the Tibetan Plateau
 1185 and Their Geodynamic Implications. *Chinese Sci Bull*, 54, 2556-2567.
- 1186 ZHANG, K.J., TANG, X.C., WANG, Y. & ZHANG, Y.X. (2011) Geochronology,
 1187 Geochemistry, and Nd Isotopes of Early Mesozoic Bimodal Volcanism in
 1188 Northern Tibet, Western China: Constraints on the Exhumation of the Central

1
2
3
4
5
6
7
8
9
10
11
12
13
14
15
16
17
18
19
20
21
22
23
24
25
26
27
28
29
30
31
32
33
34
35
36
37
38
39
40
41
42
43
44
45
46
47
48
49
50
51
52
53
54
55
56
57
58
59
60

1189 Qiangtang Metamorphic Belt. *Lithos*, 121, 167-175.

1190 ZHANG, K.J., XIA, B.D., WANG, G.M., LI, Y.T. & YE, H.F. (2004) Early
1191 Cretaceous Stratigraphy, Depositional Environments, Sandstone Provenance, and
1192 Tectonic Setting of Central Tibet, Western China. *GSA Bulletin*, 116,
1193 1202-1222.

1194 ZHANG, K.J., ZHANG, Y.X., LI, B., ZHU, Y.T. & WEI, R.Z. (2006) The
1195 Blueschist-Bearing Qiangtang Metamorphic Belt (Northern Tibet, China) as an
1196 in Situ Suture Zone: Evidence from Geochemical Comparison with the Jinsa
1197 Suture. *Geology*, 34, 493-496.

1198 ZHANG, K.J., ZHANG, Y.X., TANG, X.C. & XIA, B. (2012) Late Mesozoic
1199 Tectonic Evolution and Growth of the Tibetan Plateau Prior to the Indo-Asian
1200 Collision. *Earth-Science Reviews*, 114, 236-249.

1201 ZHANG, X.R., SHI, R.D., HUANG, Q.S., LIU, D.L., GONG, X.H., CHEN, S.S., WU,
1202 K., YI, G.D., SUN, Y.L. & DING, L. (2014) Early Jurassic High-Pressure
1203 Metamorphism of the Amdo Terrane, Tibet: Constraints from Zircon U-Pb
1204 Geochronology of Mafic Granulites. *Gondwana Research*, 26, 975-985.

1205 ZHAO, Z., BONNS, P.D., STÜBNER, K., WANG, G.-H. & EHLERS, T.A. (2017)
1206 Early Cretaceous Exhumation of the Qiangtang Terrane During Collision with
1207 the Lhasa Terrane, Central Tibet. *Terra Nova*, 29, 382-391.

1208 ZHAO, Z.B., BONNS, P.D., WANG, G.H., LIU, Y. & ZHENG, Y.L. (2014) Origin
1209 and Pre-Cenozoic Evolution of the South Qiangtang Basement, Central Tibet.
1210 *Tectonophysics*, 623, 52-66.

- 1
2
3
4 1211 ZHAO, Z., BONS, P.D., WANG, G., SOESOO, A. & LIU, Y. (2015) Tectonic
5
6 1212 Evolution and High-Pressure Rock Exhumation in the Qiangtang Terrane,
7
8 1213 Central Tibet. *Solid Earth*, 6, 457-473.
9
10
11 1214 ZHU, D.C., LI, S.M., CAWOOD, P.A., WANG, Q., ZHAO, Z.D., LIU, S.A. &
12
13 1215 WANG, L.Q. (2016) Assembly of the Lhasa and Qiangtang Terranes in Central
14
15 1216 Tibet by Divergent Double Subduction. *Lithos*, 245, 11.
16
17
18 1217 ZHU, D.C., ZHAO, Z.D., NIU, Y.L., DILEK, Y., HOU, Z.Q. & MO, X.X. (2013)
19
20 1218 The Origin and Pre-Cenozoic Evolution of the Tibetan Plateau. *Gondwana*
21
22 1219 *Research*, 23, 1429-1454.
23
24
25 1220 ZHU, T.X., QIN, J.H., ZHANG, Z.G., WANG, X.L., LUO, J.L. & ZHUANG, Z.H.
26
27 1221 (1996) The Geological Multi-Engineering of West Qiangtang Basin (Qt96yz-01),
28
29 1222 Managing Department of Tibet Oil and Gas Exploration Project, CNPC.
30
31
32 1223 ZHU, T.X., YU, Q., YONG, Y.Y., JIA, B.J., QIN, J.H., ZHANG, Z.G., WANG, X.L.,
33
34 1224 TAN, Q.Y., XIE, Y., LI, M.H., LI, Q.X. & FENG, X.C. (1997) The Tibet
35
36 1225 Petroleumgeological Survey Report (Qz-97-102101), Managing Department of
37
38 1226 Tibet Oil and Gas Exploration Project, CNPC.
39
40
41
42
43
44
45
46
47
48
49
50
51
52
53
54
55
56
57
58
59
60

Table 1 Biostratigraphy constrained by bivalves in the Quemo Co section and magnetostratigraphy

Stratigraphy	Bivalves	Biostratigraphy Age	Magnetostratigraphy Age of Fang <i>et al.</i> (2016)	Environment
Xueshan Fm.	Assemblage <i>Radulopecten fibrosus</i> - <i>Gervillella orientalis</i> - <i>Placunopsis duriuscula</i> <i>Meleagrinnella nienixionglaensis</i> Wen, <i>Radulopecten fibrosus</i> (Sowerby), <i>Miyagipecten lavisi</i> (Wen), <i>Placunopsis duriuscula</i> (Phillips), <i>P. sp.</i> , <i>Bakevillia</i> (<i>Bakevillia</i>) <i>waltoni</i> (Lycett) <i>Gervillella</i> <i>qinghaiensis</i> Wen, <i>G. orientalis</i> (Douville), <i>G. cf. siliqua</i> (Eudes-Deslongchamps), <i>Plagiostoma</i> cf. <i>channoni</i> Cox, <i>Pseudolimea duplicata</i> (Sowerby), <i>Lopha maliensis</i> Tong, <i>Modiolus</i> (<i>Modiolus</i>) <i>imbricatus</i> Sowerby, <i>Protocardia qinghaiensis</i> Wen, <i>Corbicellopsis laevis</i> (Sowerby), <i>Unicardiopsis</i> cf. <i>acesta</i> (d'Orbigny), <i>Quenstedtia</i> cf. <i>oblita</i> Greppin, <i>Q. cf. dingriensis</i> Wen, <i>Mactromya qinghaiensis</i> Wen, <i>M. gibbasa</i> (Morris et Lycett), <i>Astarte togtonheensis</i> Wen, <i>A. cf.</i> <i>elegans</i> Sowerby, <i>Tancredia triangularis</i> Wen, <i>Pseudotrapezium cordiforme</i> (Deshayes), <i>Anisocardia</i> (<i>Anisocardia</i>) <i>togtonheensis</i> Wen, <i>A. (Antiquicyprina)</i> cf. <i>trapezoidalis</i> Wen, <i>Pholadomya</i> cf. <i>carinata</i> Goldfuss, <i>Pleuromya uniformis</i> (Sowerby), <i>Playtmyoidea</i> sp.	Kimmeridgian	<157.5 Ma	Marine
Suowa Fm.	Assemblage <i>Myopholas multicostata</i> - <i>Placunopsis duriuscula</i> - <i>Camptonectes</i> (<i>Camptonectes</i>) <i>auritus</i> <i>Palaeonucula</i> sp., <i>Mesosacella morrissi</i> (Deshayes), <i>M. wenquanensis</i> Sha, Fursich, Smith et Wang, <i>Nuculana</i> (<i>Praesacella</i>) cf. <i>ovum</i> (Sowerby), <i>Grammatodon</i> (<i>Grammatodon</i>) cf. <i>clathratum</i> (Leckenby), <i>Pinna</i> sp., <i>Meleagrinnella</i> sp., <i>Pteria</i> cf. <i>plana</i> (Morris et Lycett), <i>Miyagipecten laevis</i> (Wen), <i>Radulopecten tipperi</i> Cox, <i>R. vagans</i> (Sowerby), <i>R. tripartitus</i> Sha, Fursich, Smith et Wang, <i>R. fibrosus</i> (Sowerby), <i>R. pamirensis</i> Wen, <i>R. gerzensis</i> Wen, <i>Camptonectes</i> (<i>Camptonectes</i>) <i>auritus</i> (Schlotheim), <i>C. (C.) laminatus</i> (Sowerby), <i>C. (Camptochlamys) clathratus</i> (Roemer), <i>C. (Annulinectes) obscurus</i> (Sowerby), <i>Propeamussium</i> (<i>Propeamussium</i>) cf. <i>pumilum</i> (Lamarck), <i>Placunopsis</i> cf. <i>subelongata</i> (d'Orbigny), <i>Placunopsis</i> cf. <i>socialis</i> Morris et Lycett, <i>P.</i> <i>duriuscula</i> (Phillips), <i>Gervillella qinghaiensis</i> Wen, <i>G. siliqua</i> (Eudes-Deslongchamps), <i>G. sp.</i> , <i>Bakevillia?</i> sp., <i>Aguilerella</i> sp., <i>Pseudolimea duplicata</i> (Sowerby), <i>P. tjubegatanica</i> (Repman), <i>P.</i> sp., <i>Plagiostoma</i> cf. <i>channoni</i> Cox, <i>Lopha</i> cf. <i>tifoensis</i> Cox, <i>L. cf. maliensis</i> Tong, <i>Liostrea</i> cf. <i>jiangjinensis</i> Wen, <i>L. cf. birmanica</i> (Reed), <i>L. cf. blanfordi</i> Cox, <i>Plicatula</i> sp., <i>Modiolus</i> (<i>Modiolus</i>) <i>imbricatus</i> Sowerby, <i>M. (M.)</i> cf. <i>trigonus</i> Chen, <i>Myophorella?</i> sp., <i>Protocardia stricklandi</i> (Morris et Lycett), <i>P. qinghaiensis</i> Wen, <i>Mactromya</i> cf. <i>qinghaieusis</i> Wen, <i>Astarte togtonheensis</i> Wen, <i>A.</i> cf. <i>elegans</i> Sowerby, <i>A. cf. maliensis</i> Tong, <i>Astartoides gambaensis</i> Wen et Lan, <i>A. cf. dingriensis</i> Wen, <i>Anisocardia</i> (<i>Anisocardia</i>) <i>rostrata</i> (Sowerby), <i>A. (A.)</i> cf. <i>channoni</i> Cox, <i>A. (A.) togtonheensis</i> Wen, <i>A. (A.)</i> sp., <i>A. (Antiquicyprina)</i> cf. <i>trapezoidalis</i> Wen, <i>Pseudotrapezium cordiforme</i> (Deshayes), <i>Amiodon fengdengensis</i> (Chen), <i>A. cf. khoratensis</i> (Hayami), <i>Platymyoidea</i> sp., <i>Myopholas multicostata</i> (Agassiz), <i>M. percostata</i> Douville, <i>Pleuromya</i> cf. <i>uniformis</i> (Sowerby), <i>P.</i> <i>subelongata</i> (d'Orbigny), <i>P. sp.</i>	Callovian- Oxfordian	160.1-<157.5 Ma	Marine
Xiali Fm.	Assemblage <i>Pteroperna costatula</i> — <i>Radulopecten vagans</i> <i>Palaeonucula</i> sp., <i>Pinna?</i> sp., <i>Meleagrinnella</i> cf. <i>braamburiensis</i> (Phillips), <i>Radulopecten tipperi</i> Cox, <i>R. vagans</i> (Sowerby), <i>R. pamirensis</i> Wen, <i>R. sp.</i> , <i>Placuopsis duriuscula</i> (Phillips), <i>Bakevillia</i> (<i>Bakevillia</i>) <i>waltoni</i> (Lycett), <i>Gervillella qinghaiensis</i> Wen, <i>Costigervillia minima</i> Wen, <i>Lopha</i> cf. <i>tifoensis</i> Cox, <i>Liostrea jiangjinensis</i> Wen, <i>Pteria plana</i> Roemer, <i>Pteroperna costatula</i> (Deslongchamps), <i>P. sp.</i> , <i>Modiolus</i> (<i>Modiolus</i>) <i>imbricatus</i> Sowerby, <i>Yanguonia</i> cf. <i>yanshipingensis</i>	Bathonian- Callovian	163.3-160.1 Ma	Marine

	Wen, <i>Protocardia</i> (<i>P.</i>) <i>qinghaiensis</i> Wen, <i>P.</i> (<i>P.</i>) <i>stricklandi</i> (Morris et Lycett), <i>Corbicellopsis</i> cf. <i>laevis</i> (Sowerby), <i>Unicardiopsis amdoensis</i> Wen, <i>Corbula yanshipingensis</i> Wen, <i>C. kidugalloensis</i> Cox, <i>C. sp.</i> , <i>Astarte</i> cf. <i>elegans</i> Sowerby, <i>A. sp.</i> , <i>Anisocardia</i> (<i>Anisocardia</i>) cf. <i>channoni</i> Cox, <i>A. (A.) rostrata</i> (Sowerby), <i>Pseudotrapezium cordiforme</i> (Deshayes), <i>Amiodon</i> cf. <i>choratensis</i> (Hayami), <i>Thracia togtonheensis</i> Wen			
Buqu Fm.	Assemblage <i>Isognomon</i> (<i>Mytiloperna</i>) <i>bathonicus</i> - <i>Protocardia hepingxiangensis</i> - <i>Praeexogyra</i> cf. <i>acaminata</i> <i>Liostrea birmanica</i> , <i>Ceratomya undalat</i> , <i>C. concentrica</i> , <i>Grammatodon</i> (<i>Grammatodon</i>) <i>clathratum</i> , <i>Pinna tibetica</i> , <i>P. nyainrongensis</i> , <i>Radulopecten tipperi</i> , <i>Protocardia hepingxiangensis</i> , <i>Liostrea jiangjinensis</i> , <i>L. zadoensis</i> , <i>Lopha maliensis</i> , <i>L. baqenensis</i> , <i>Entolium nienixionglaensis</i> , <i>Praeexogyra</i> cf. <i>acaminata</i> , <i>Radulopecten shuanghuensis</i> , <i>Gervillella qinghaiensis</i> , <i>Pteria problematica</i> , <i>Modiolus</i> (<i>Modiolus</i>) <i>trigonus</i> , <i>Mactromya qinghaiensis</i> , <i>Neomiodon yanshipingensis</i> , <i>A. (Antiquicyprina)</i> <i>trapezoidalis</i> , <i>Pholadomya socialis qinghaiensis</i>	Bathonian	165.5-163.3 Ma	Marine
Quemocuo Fm.	<i>Quenstedtia?</i> <i>sp.</i> Assemblage <i>Undulatula perlonga</i> - <i>Psilunio chaoi</i> <i>Psilunio chaoi</i> Grabau, <i>P. lateriplanus</i> Ma, <i>P. thailandicus</i> (Hayami), <i>P. sinensis</i> Gu, <i>Lamprotula</i> (<i>Eolamprotula</i>) <i>sp.</i> , <i>Undulatula perlonga</i> Gu, <i>U. ptychorhyncha</i> Gu, <i>Cuniopsis</i> cf. <i>johannisbohmi</i> (Frech), <i>Soleniaa tanggulaensis</i> Wen, <i>Unio</i> cf. <i>obrustschewi</i> Martinson, <i>Margaritifera isfarensis</i> Chernyshev	Bajocian	>171.2-165.5 Ma	Marine Fresh water
Erlongba Fm.	Assemblage <i>Amonotis togtonheensis</i> - <i>Cardium</i> (<i>Tulongocardium</i>) <i>xizhangensis</i>	Norian- Rhaetian	212±1.7 Ma (Volcanics, Bai et al., 2005)	
Bagong Fm.	Assemblage <i>Halobia superbescens</i> - <i>H. disperseinsecta</i> Assemblage <i>Amonotis togtonheensis</i> - <i>Cardium</i> (<i>Tulongocardium</i>) <i>xizhangensis</i>	Norian		
Bolila Fm.	<i>Cassianella</i> cf. <i>berychi</i> , <i>Halobia plicosa</i> , <i>H. superbescens</i> , <i>H. sp.</i> , <i>Plagiostoma sp.</i>	Carnian		

Bivalves are from Geological report of the 1:250, 000 regional geological survey in Chibuzhang Co area.

Table 2 Apatite fission track data for the Qiangtang Basin

Sample	Stratigraphy	ρ_s ^a	N_s ^b	ρ_i ^a	N_i ^b	ρ_d ^a	N_d ^b	$P(\chi^2)$ ^c	D_{par} ^d	$[U]$ ^e	Central age ^f	$\pm 1\sigma$	Dis. ^g	N_c ^h	MTL	$\pm 1\sigma$	N_c ⁱ
		(10 ⁵ cm ⁻²)		(10 ⁵ cm ⁻²)		(10 ⁵ cm ⁻²)			(μ m)	(ppm)	(Ma)	(%)	(μ m)				
D0609	J ₂ x	9.418	728	12.903	1152	12.4	8749	1.00	2.65	17.91	113.6	5.4	0	30	12.17	0.36	20
D0815	J ₂ x	10.0	148	27.365	405	12.3	8749	0.54	2.84	30.46	65.4	6.3	0	9	/	/	/
ED0616	J ₂ x	5.403	667	10.726	1324	12.0	8749	0.00	2.00	12.15	90.7	6.8	28	27	11.70	0.31	29
ED0620	T ₃ d	4.468	652	14.281	2084	12.0	8749	0.24	1.98	15.54	55	2.5	4.7	32	11.71	0.56	28
EP1502	J ₂ x	4.508	702	14.456	2251	12.2	8749	0.00	2.23	16.84	55.6	3.7	25	28	10.84	0.44	29
EP1503	J ₂ b	4.775	609	19.247	2445	12.1	8749	0.14	2.20	22.7	44.6	2.3	14	30	9.26	0.39	31
EP1504-09	K ₂ a	5.256	1048	18.776	3744	12.1	8749	0.23	2.55	19.54	49.1	2	10	40	13.4	0.45	15
EP1504-17	K ₂ a	5.848	576	17.188	1693	12.0	8749	0.03	3.49	18.01	62.5	4.2	17	18	14.54	0.32	5
EP1505	T ₃ d	7.043	836	23.361	2773	12.2	8749	0.40	2.40	28.59	53.7	2.4	9.2	32	12.87	0.29	22
EP1506	T ₃ d	9.154	638	19.283	1344	12.2	8749	0.93	2.48	22.32	84.1	4	0	30	13.75	0.48	17

PQ1503	J_2q	4.492	549	15.921	1946	11.3	6621	0.00	1.74	17.11	40.1	2.6	23	30	12.59	0.14	101
PQ1506	J_2x	9.082	801	12.492	1190	12.4	8749	100	2.15	16.52	120.9	5.5	0	32	12.01	0.22	37

^a p_s , p_i , p_d are track densities of spontaneous, induced and dosimeter tracks.

^b N_s , N_i , N_d are the number of spontaneous, induced and dosimeter tracks.

^c $P(\chi^2)$ is the value of chi-square test (Galbraith, 1981; Green, 1981).

^d D_{par} is the etch pit diameter, which is used as a proxy for the influence of chemical composition on track annealing (Donelick *et al.*, 2005).

^e Uranium content calculated with TrackKey (Dunkl, 2002).

^f Central ages are calculated using TrackKey (Dunkl, 2002) with 1σ standard error. Ages are calculated with a $\zeta=292.4\pm17.9$ for a standard IRMM540 glass.

^g Dispersion is the standard deviation of the true single-grain ages as a percentage of their central age (Galbraith, 2005).

^h N_c is the number of grains counted for age calculation.

ⁱ N_c is the number of measured horizontal confined tracks.

1
2
3
4
5
6
7
8
9
10
11
12
13
14
15
16
17
18
19
20
21
22
23
24
25
26
27
28
29
30
31
32
33
34
35
36
37
38
39
40
41
42
43
44
45
46
47
48
49
50
51
52
53
54
55
56
57
58
59
60

Figure legends:

Fig. 1. a, Major terranes and sutures of the Tibetan plateau. b, Geological map of Qiangtang basin and adjacent terranes (modified after Kapp *et al.*, 2005). WK-ATSZ = West Kunlun-Altyn Tagh suture zone; SKSZ = South Kunlun suture zone; CQMB = Central Qiangtang metamorphic belt; JRSZ = Jinsha River suture zone; BNSZ = Bangong-Nujiang suture zone. Numbers in grey stars represent the localities of composite sections: 1, Duxue Mt.; 2, Shuangquan Lake; 3, Heihuling; 4, Nadigangri; 5, Changshui River; 6, Amugang; 7, Zuerkenwula Mt.; 8, Dangmagang; 9, Quemo Co; 10, Biluo Co; 11, Dazhuoma.

Fig. 2. Correlation of sequences, lithologies and paleo-environments of main Mesozoic stratigraphic units of the Qiangtang Basin. Not drawn to scale. The lithologies and interpretations of depositional environment of both the North and South Qiangtang are from field observations and geological reports. The age of Nadigangri Fm. comes from Zhai & Li (2007), Wang et al. (2008b) and Fu et al. (2010). Ages of Jurassic sequences are from magnetostratigraphy of Fang et al. (2016). The age of Abushan Fm. is from Li et al. (2015c). The legend of lithology is same to that of Fig. 4. All symbols are filled using patterns provided by U.S. Geological Survey (2006).

Fig. 3. Remote sensing images of specific profiles of continuous successions in Nadigangri (a) and Quemo Co (b) from Google Earth©. Structural dips are labelled

1249 on the strata. The solid lines are boundaries between stratigraphic units. The yellow
 1250 dashed lines represent unconformities. T_3nd = Nadigangri Formation; T_3b = Bolila
 1251 Formation; T_3bg = Bagong Formation; T_3e = Erlongba Formation; J_2q = Quemocuo
 1252 Formation; J_2b = Buqu Formation; J_2x = Xiali Formation; J_3s = Suowa Formation; J_3b
 1253 = Bailongbinghe Formation; J_3K_1x = Xueshan Formation; E_2k = Kangtuo Formation.

1254

1255 Fig. 4. Simplified stratigraphic framework of nine composite sections in the North
 1256 Qiangtang sub-basin. The stratigraphic codes are same to those of Fig. 3. Other codes
 1257 are: $P_{1-2}l$ = Lugu Formation; T_3j = Juhuashan Formation; T_3z = Zangxiahe Formation;
 1258 T_3T = Tumengela Group; E_2s = Suonahu Formation; $E_{1-2}t$ = Tuotuohe Formation;
 1259 $E_{2+3}y$ = Yulinshan Formation; N_1c = Chabaoma Formation; N_2q = Quguo Formation;
 1260 N_2sq = Shuangquanhu Formation.

1261

1262 Fig. 5. Simplified stratigraphic framework of two composite sections in the South
 1263 Qiangtang sub-basin. The legend, scale and stratigraphic codes are same to those of
 1264 Fig. 4. Other codes are: T_3a = Adula Formation; T_3d = Duogaila Formation; T_3R =
 1265 Riganpeicuo Group; T_3J_1s = Suobucha Formation; J_1q = Quse Formation; J_2s = Sewa
 1266 Formation; K_2a = Abushan Formation.

1267

1268 Fig. 6. Decompaction scheme (modified after Allen and Allen, 2005).

1269

1270 Fig. 7. Specific indicators for assessment of paleo-water depth in stratigraphic

1
2
3
4 1271 sections. (a) Oscillatory ripples preserved in the bottom of tidal sandstones (Late
5
6 1272 Triassic Duogaila Formation, Dazhuoma; paleo-water depth $\approx 50\pm 50$ m). (b)
7
8
9 1273 Fining-upward sequence with each starting with conglomerate or pebbled sandstones
10
11 1274 (Middle Jurassic Quemocuo Formation, Amugang; paleo-water depth $\approx 10\pm 10$ m). (c)
12
13
14 1275 Current bedding limestone (Middle Jurassic Quemocuo Formation, Amugang;
15
16 1276 paleo-water depth $\approx 50\pm 50$ m). (d) Ripples in tidal sandstones (Middle Jurassic Xiali
17
18
19 1277 Formation, Dazhuoma; paleo-water depth $\approx 50\pm 50$ m). (e) Ammonite in mudstone
20
21
22 1278 (Late Jurassic Bailongbinghe Formation, Changshui River; paleo-water depth ≈ 50 m).
23
24
25 1279 (f) Directional arrangement of gravels in fluvial sandstones (Late Cretaceous Abushan
26
27 1280 Formation, Biluo Co; paleo-water depth $\approx 10\pm 5$ m).
28
29
30 1281

31
32
33 1282 Fig. 8. Subsidence curves for composite sections in Fig. 1. The thick solid line
34
35 1283 represents backstripped tectonic subsidence. The thin solid line represents total
36
37 1284 decompacted subsidence. The grey-shade areas represent the first stage of subsidence
38
39
40 1285 from Late Triassic to Early Jurassic based on the subsidence histories, combined with
41
42 1286 previous work on sediment provenance and timing of deformation. The reference
43
44
45 1287 lines representing subsidence rate are shown are each of the plots.
46
47
48 1288

49
50
51 1289 Fig. 9. Magnification of the tectonic subsidence histories from 172 to 120 Ma. The
52
53 1290 reference lines representing subsidence rate are shown are each of the plots. The
54
55 1291 shaded area represent the gradual cessation of subsidence across the Qiangtang Basin,
56
57
58 1292 with the final termination at about 148 Ma. The subsidence curves in the North
59
60

Qiangtang are represented by solid lines, while the South Qiangtang are represented by dotted lines.

Fig. 10. Radial plots of detrital apatite fission track ages in the Qiangtang Basin using DensityPlotter (Vermeesch, 2012).

Fig. 11. Weighted mean thermal paths for sandstones in the Qiangtang Basin. The mélange and granite samples are from the Central Uplift studied by Zhao *et al.* (2017). All thermal paths display cooling starting from 150-130 Ma. The depth is calculated by assuming a geothermal gradient of 20 °C/km.

Fig. 12. Schematic map showing the paleo-current directions, provenance areas and composition of lithic fragments in sandstones of the Qiangtang foreland basin during the Middle Jurassic to Early Cretaceous time, modified from Li *et al.* (2001).

Fig. 13. Cartoon of tectonic evolution of the Qiangtang Basin and adjacent terranes from Late Triassic to Cretaceous. The extent of each terrane is not strictly to scale and the near surface geometries are vertically exaggerated. The evolution models of **Central Uplift** during early Late Triassic (a) and Late Triassic-Early Jurassic (b) are modified after Zhang & Tang (2009). Bold black arrows in each cross sections represent the directions of sediment transportation. The mechanisms of subsidence are labelled in red.

1		
2		
3		
4	1315	
5		
6	1316	Supporting material legends
7		
8		
9	1317	File S1 Stratigraphic sections in the Qiangtang Basin in Google Earth format.
10		
11	1318	Table S1 Stratigraphic data of eleven composite sections in Qiangtang basin
12		
13		
14	1319	Table S2 Age constraints from biostratigraphy of strata in Qiangtang basin
15		
16		
17	1320	Table S3 GPS coordinates of AFT samples
18		
19		
20	1321	Figure S1. Thermal history modeling results of samples from the Qiangtang Basin
21		
22		
23		
24		
25		
26		
27		
28		
29		
30		
31		
32		
33		
34		
35		
36		
37		
38		
39		
40		
41		
42		
43		
44		
45		
46		
47		
48		
49		
50		
51		
52		
53		
54		
55		
56		
57		
58		
59		
60		

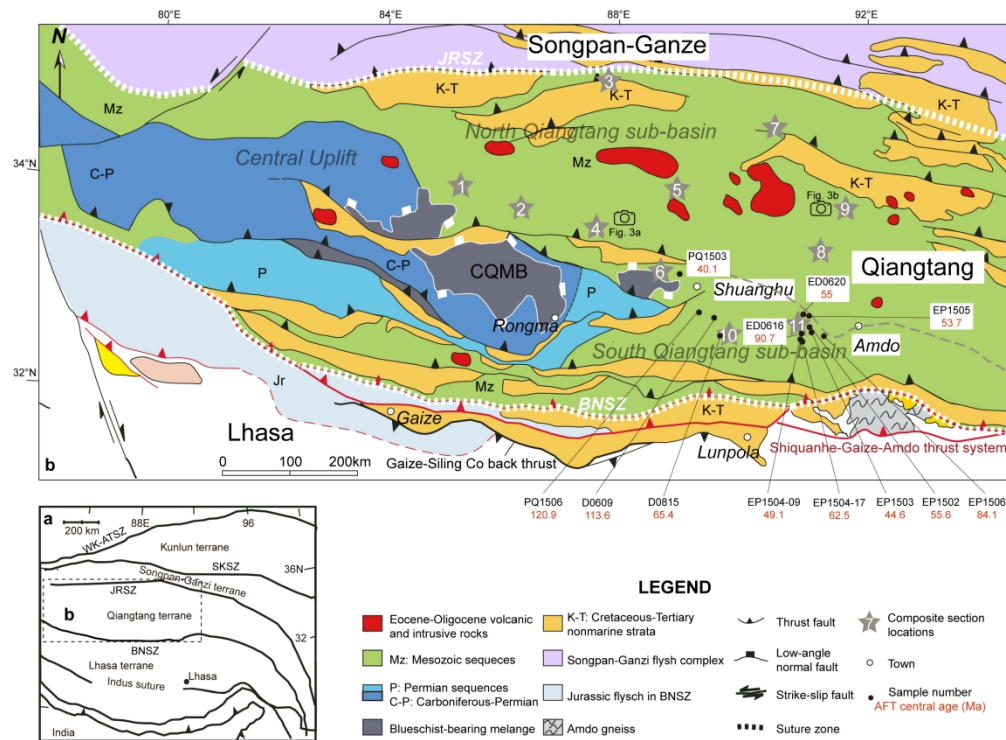


Fig. 1. a, Major terranes and sutures of the Tibetan plateau. b, Geological map of Qiangtang basin and adjacent terranes (modified after Kapp et al., 2005). WK-ATSZ = West Kunlun-Altyr Tagh suture zone; SKSZ = South Kunlun suture zone; CQMB = Central Qiangtang metamorphic belt; JRSZ = Jinsha River suture zone; BNSZ = Bangong-Nujiang suture zone. Numbers in grey stars represent the localities of composite sections: 1, Duxue Mt.; 2, Shuangquan Lake; 3, Heihuling; 4, Nadigangri; 5, Changshui River; 6, Amugang; 7, Zuerkenwula Mt.; 8, Dangmagang; 9, Quemo Co; 10, Biluo Co; 11, Dazhuoma.

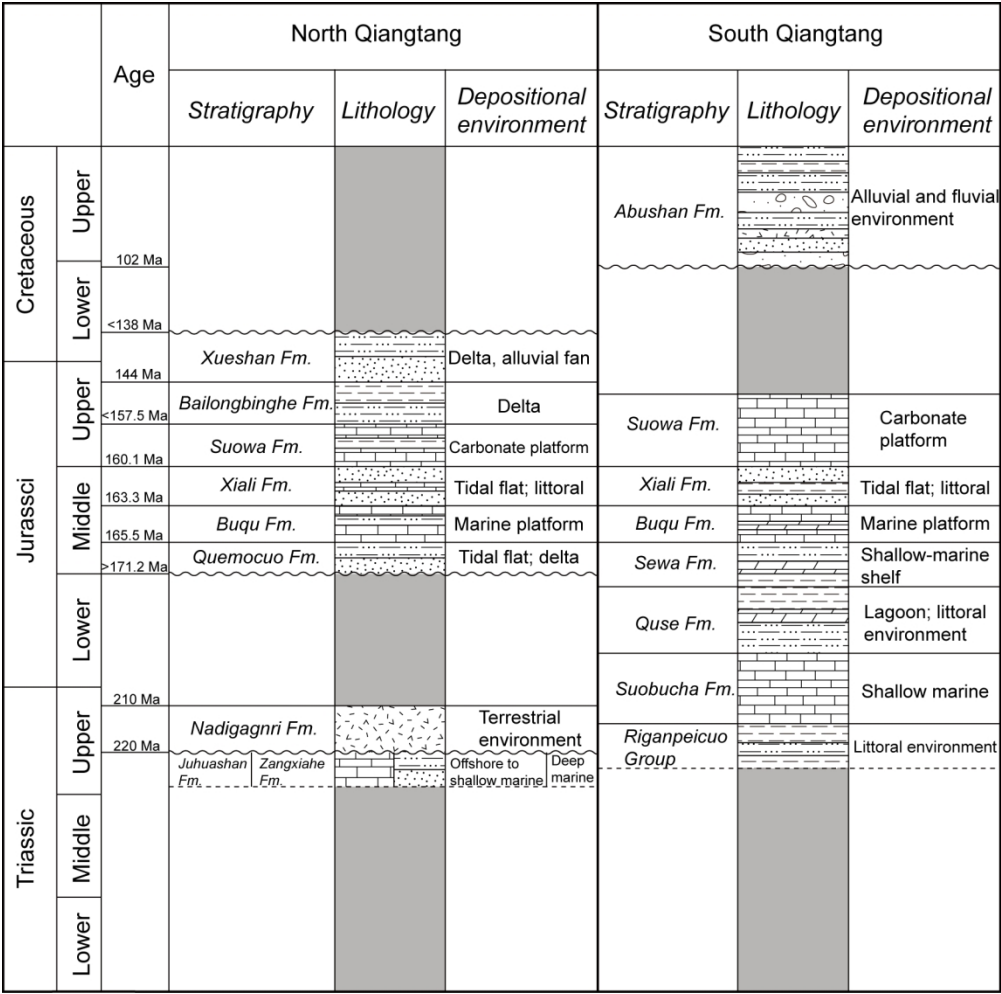


Fig. 2. Correlation of sequences, lithologies and paleo-environments of main Mesozoic stratigraphic units of the Qiangtang Basin. Not drawn to scale. The lithologies and interpretations of depositional environment of both the North and South Qiangtang are from field observations and geological reports. The age of Nadigangri Fm. comes from Zhai & Li (2007), Wang et al. (2008b) and Fu et al. (2010). Ages of Jurassic sequences are from magnetostratigraphy of Fang et al. (2016). The age of Abushan Fm. is from Li et al. (2015c). The legend of lithology is same to that of Fig. 4. All symbols are filled using patterns provided by U.S. Geological Survey (2006).

151x149mm (300 x 300 DPI)

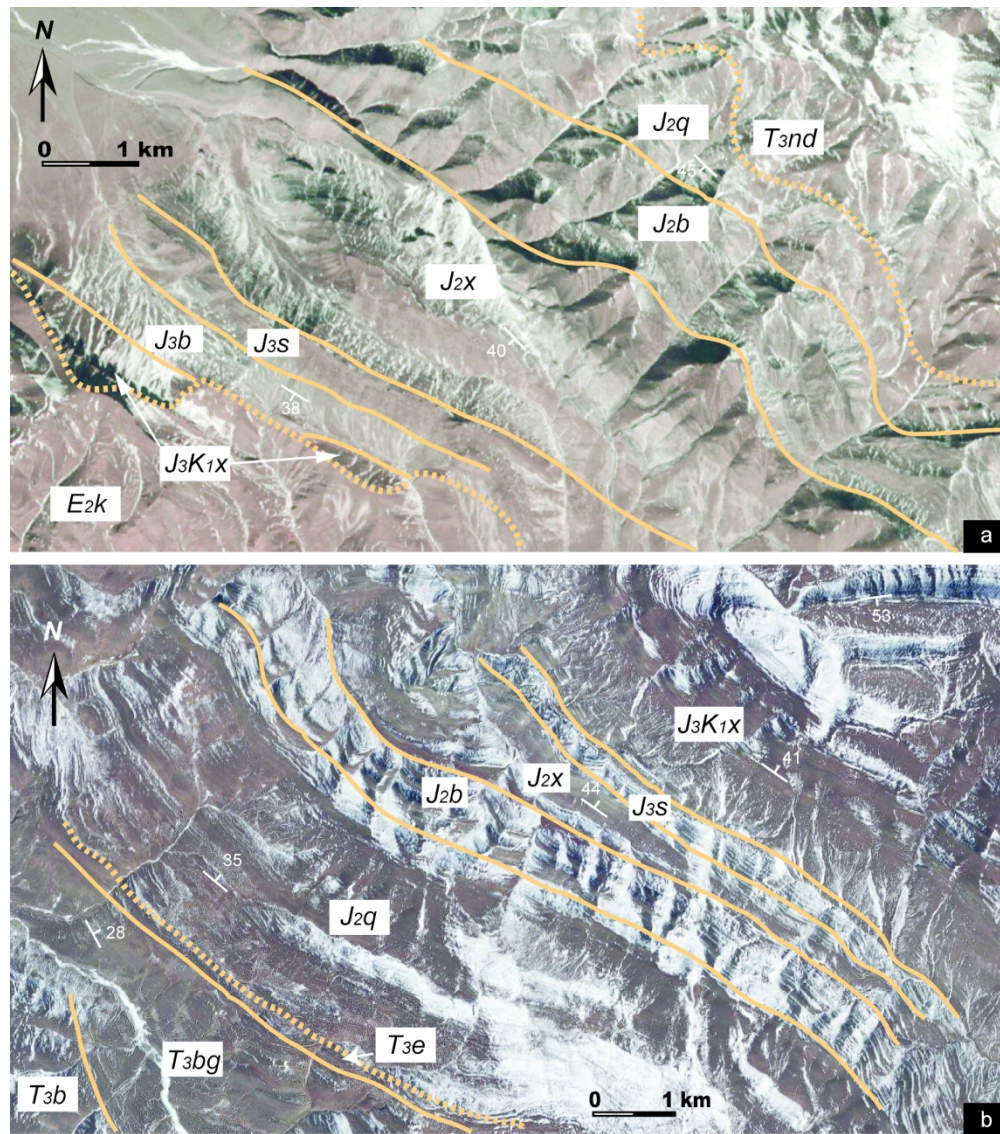


Fig. 3. Remote sensing images of specific profiles of continuous successions in Nadigangri (a) and Quemo Co (b) from Google Earth©. Structural dips are labelled on the strata. The solid lines are boundaries between stratigraphic units. The yellow dashed lines represent unconformities. T3nd = Nadigangri Formation; T3b = Bolila Formation; T3bg = Bagong Formation; T3e = Erlongba Formation; J2q = Quemocuo Formation; J2b = Buqu Formation; J2x = Xiali Formation; J3s = Suowa Formation; J3b = Bailongbinghe Formation; J3K1x = Xueshan Formation; E2k = Kangtuo Formation.

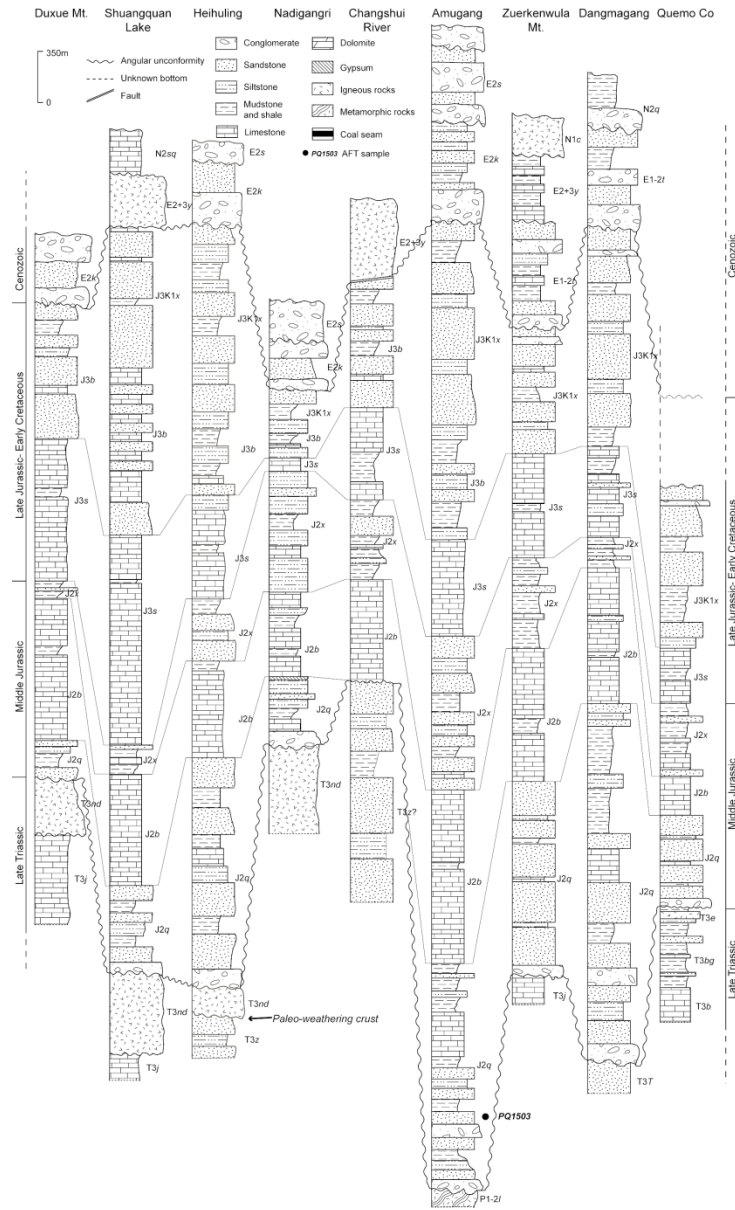


Fig. 4. Simplified stratigraphic framework of nine composite sections in the North Qiangtang sub-basin. The stratigraphic codes are same to those of Fig. 3. Other codes are: P1-2l = Lugu Formation; T3j = Juhuashan Formation; T3z = Zangxiahe Formation; T3T = Tumengela Group; E2s = Suonahu Formation; E1-2t = Tuotuohe Formation; E2+3y = Yulinshan Formation; N1c = Chabaoma Formation; N2q = Quguo Formation; N2sq = Shuangquanhu Formation.

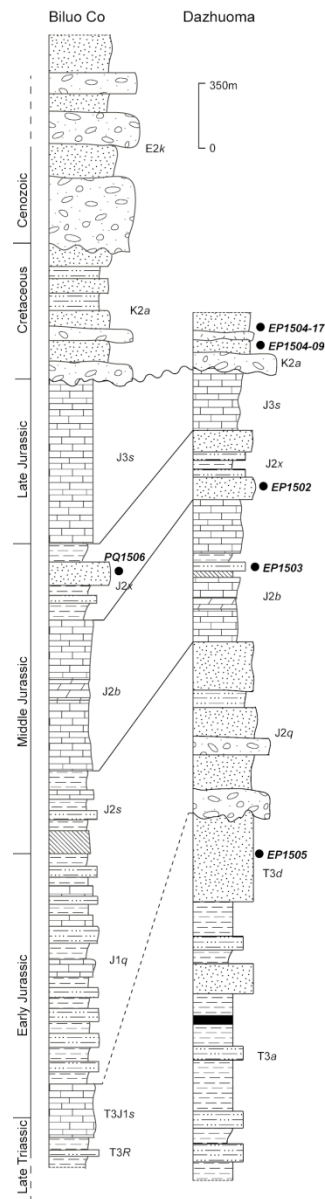


Fig. 5. Simplified stratigraphic framework of two composite sections in the South Qiangtang sub-basin. The legend, scale and stratigraphic codes are same to those of Fig. 4. Other codes are: T3a = Adula Formation; T3d = Duogaila Formation; T3R = Riganpeicuo Group; T3J1s = Suobucha Formation; J1q = Quse Formation; J2s = Sewa Formation; K2a = Abushan Formation.

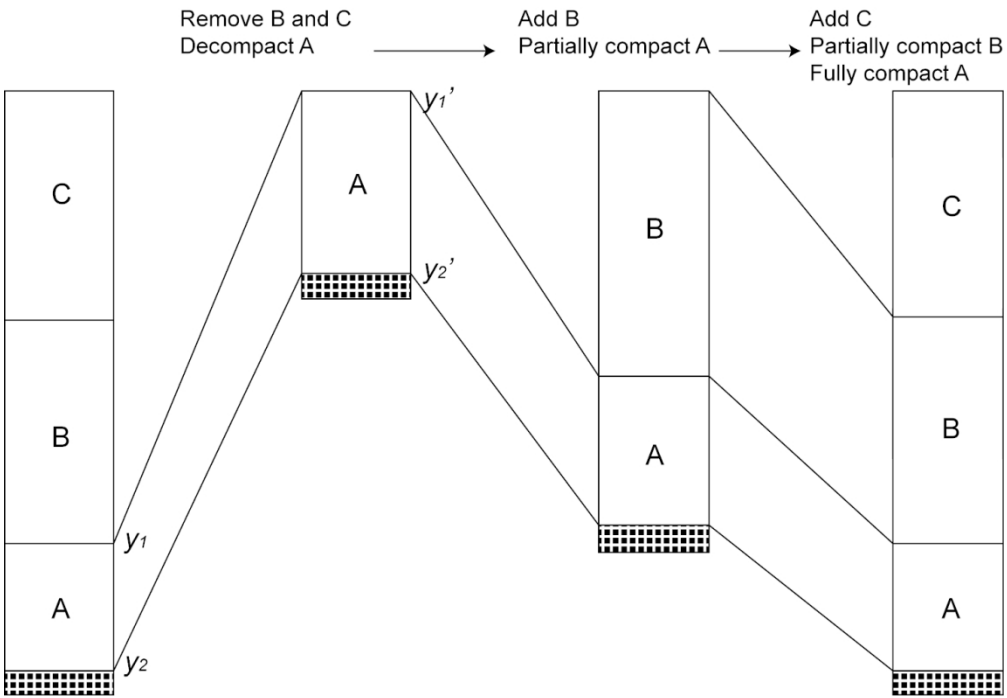


Fig. 6. Decompaction scheme (modified after Allen and Allen, 2005).



Fig. 7. Specific indicators for assessment of paleo-water depth in stratigraphic sections. (a) Oscillatory ripples preserved in the bottom of tidal sandstones (Late Triassic Duogaila Formation, Dazhuoma; paleo-water depth $\approx 50 \pm 50$ m). (b) Fining-upward sequence with each starting with conglomerate or pebbled sandstones (Middle Jurassic Quemocuo Formation, Amugang; paleo-water depth $\approx 10 \pm 10$ m). (c) Current bedding limestone (Middle Jurassic Quemocuo Formation, Amugang; paleo-water depth $\approx 50 \pm 50$ m). (d) Ripples in tidal sandstones (Middle Jurassic Xiali Formation, Dazhuoma; paleo-water depth $\approx 50 \pm 50$ m). (e) Ammonite in mudstone (Late Jurassic Bailongbinghe Formation, Changshui River; paleo-water depth ≈ 50 m). (f) Directional arrangement of gravels in fluvial sandstones (Late Cretaceous Abushan Formation, Biluo Co; paleo-water depth $\approx 10 \pm 5$ m).

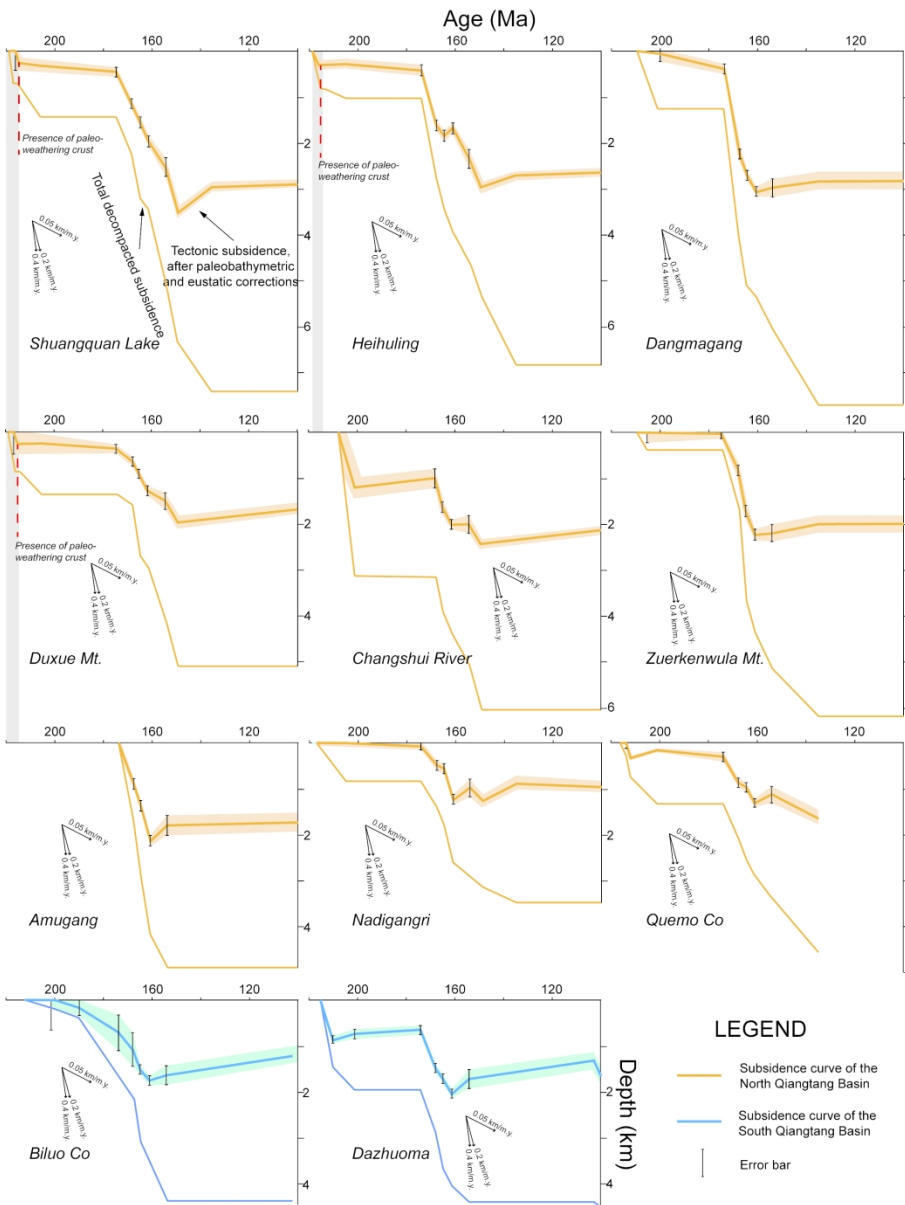


Fig. 8. Subsidence curves for composite sections in Fig. 1. The thick solid line represents backstripped tectonic subsidence. The thin solid line represents total decompacted subsidence. The grey-shade areas represent the first stage of subsidence from Late Triassic to Early Jurassic based on the subsidence histories, combined with previous work on sediment provenance and timing of deformation. The reference lines representing subsidence rate are shown are each of the plots.

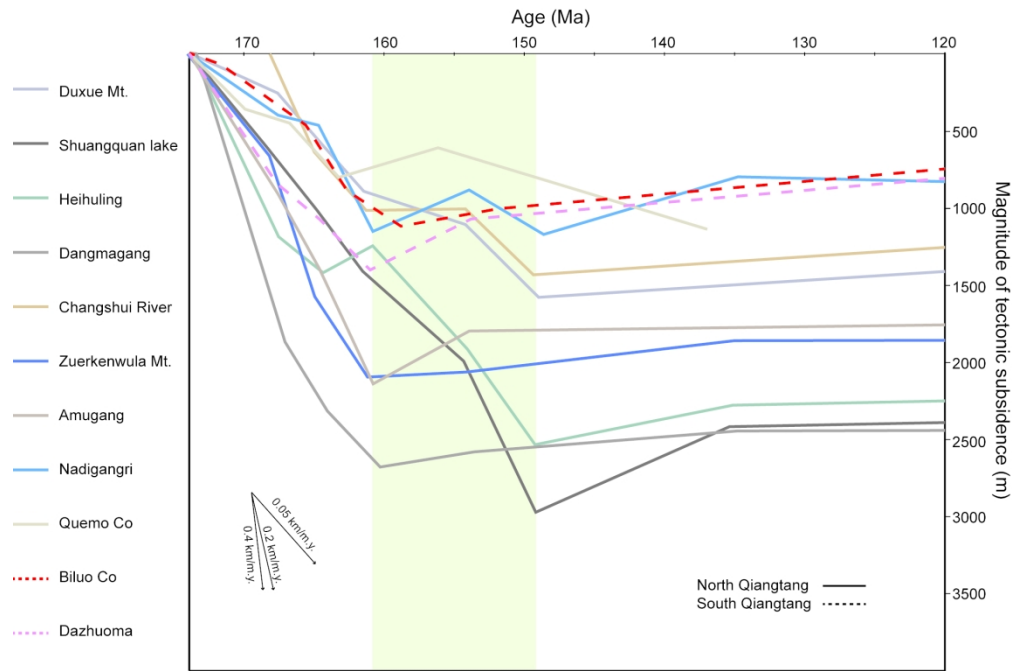


Fig. 9. Magnification of the tectonic subsidence histories from 172 to 120 Ma. The reference lines representing subsidence rate are shown are each of the plots. The shaded area represent the gradual cessation of subsidence across the Qiangtang Basin, with the final termination at about 148 Ma. The subsidence curves in the North Qiangtang are represented by solid lines, while the South Qiangtang are represented by dotted lines.

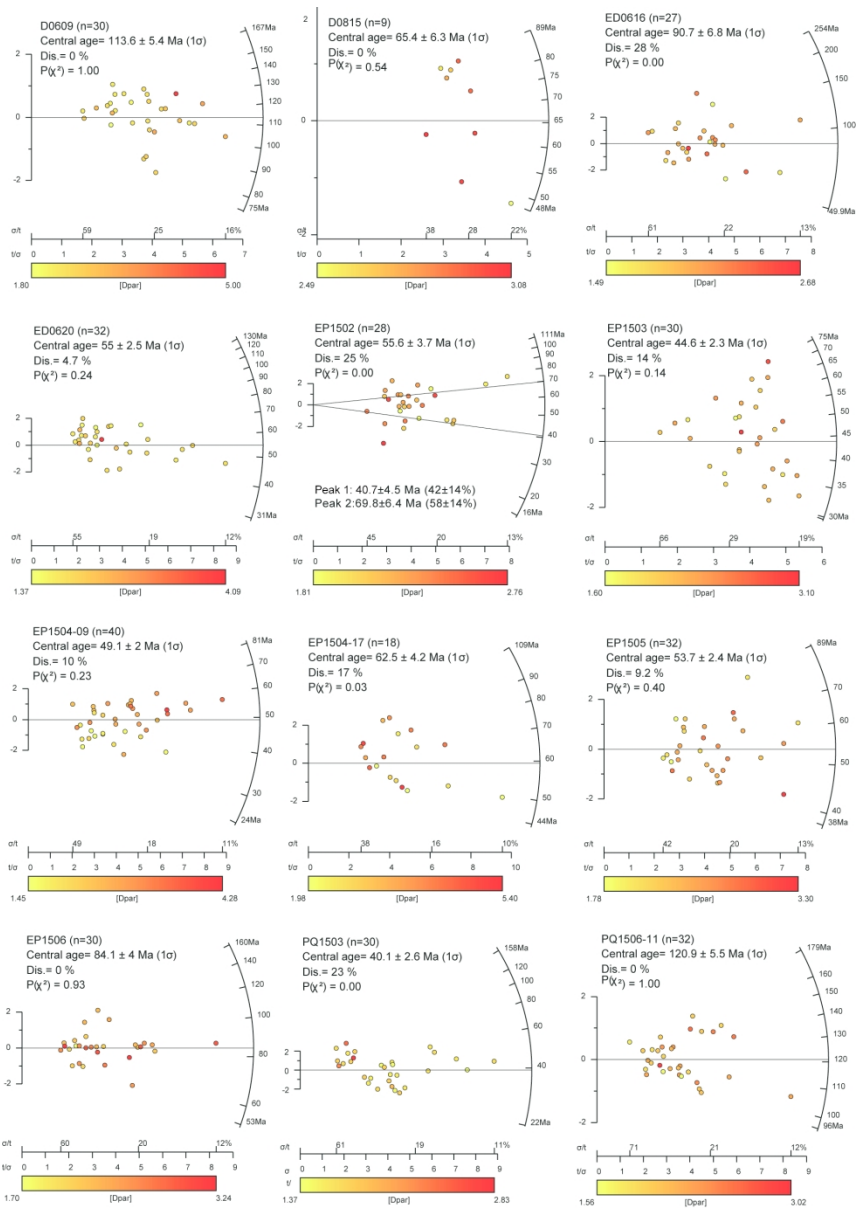


Fig. 10. Radial plots of detrital apatite fission track ages in the Qiangtang Basin using DensityPlotter (Vermeesch, 2012).

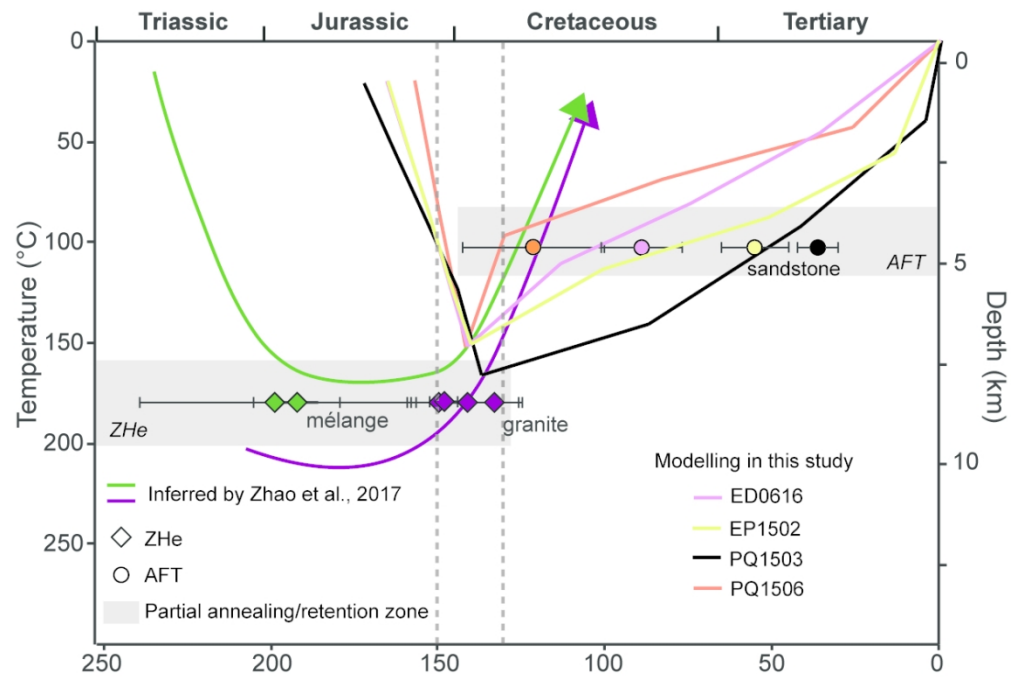


Fig. 11. Weighted mean thermal paths for sandstones in the Qiangtang Basin. The *mélange* and granite samples are from the Central Uplift studied by Zhao et al. (2017). All thermal paths display cooling starting from 150-130 Ma. The depth is calculated by assuming a geothermal gradient of 20 °C/km.

104x70mm (300 x 300 DPI)

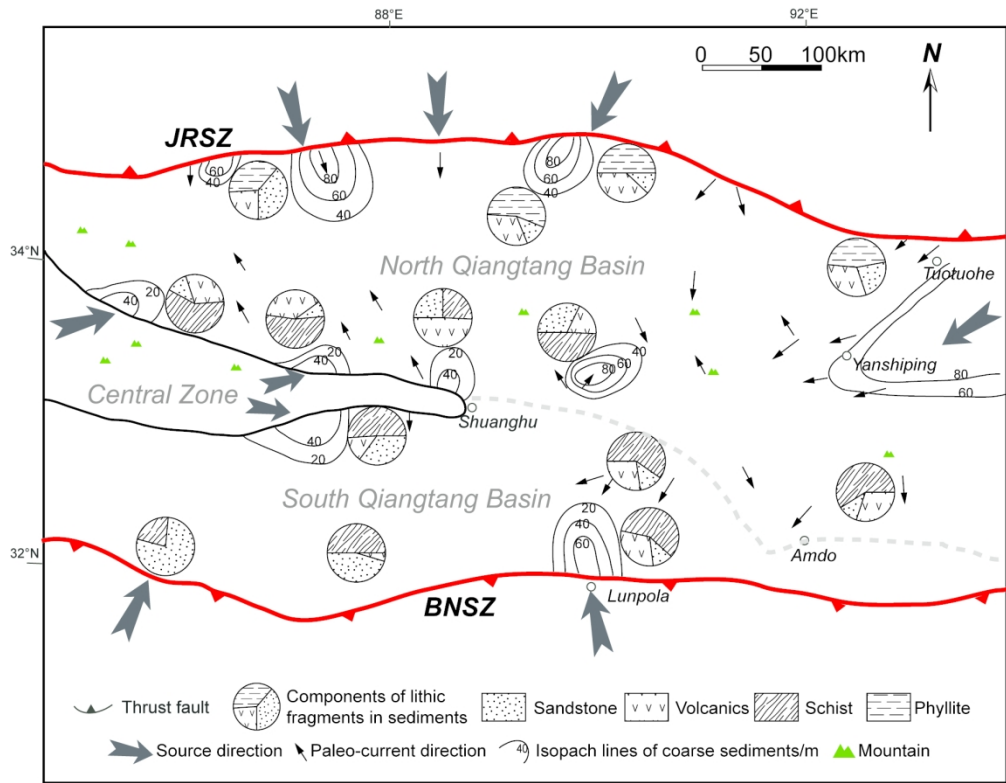


Fig. 12. Schematic map showing the paleo-current directions, provenance areas and composition of lithic fragments in sandstones of the Qiangtang foreland basin during the Middle Jurassic to Early Cretaceous time, modified from Li et al. (2001).

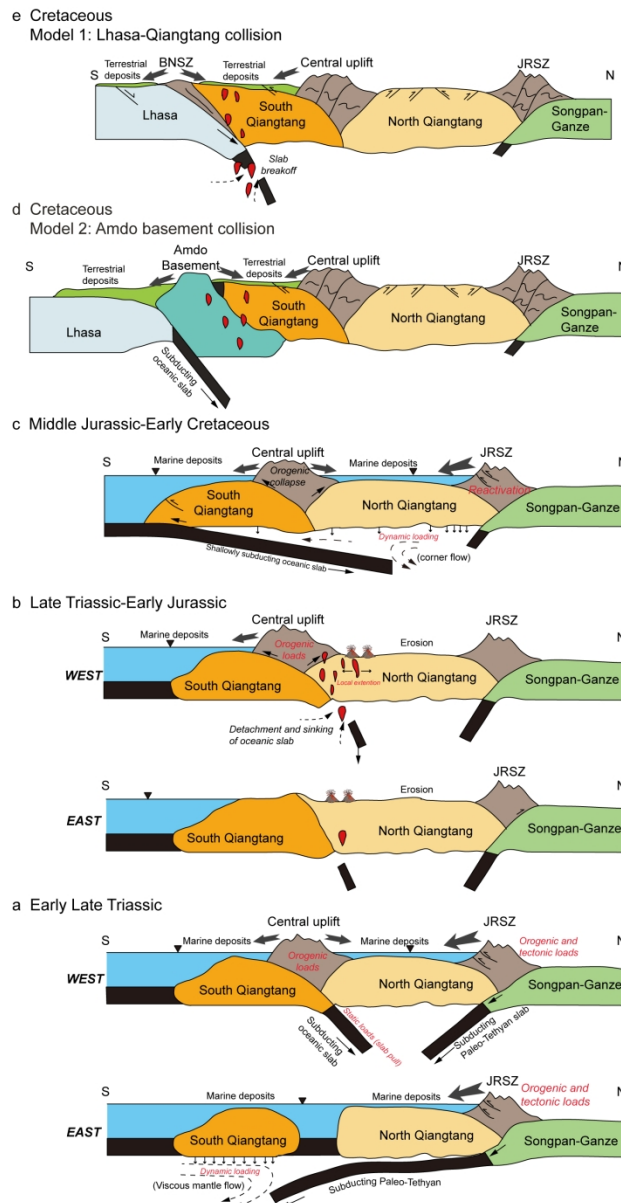


Fig. 13. Cartoon of tectonic evolution of the Qiangtang Basin and adjacent terranes from Late Triassic to Cretaceous. The extent of each terrane is not strictly to scale and the near surface geometries are vertically exaggerated. The evolution models of Central Uplift during early Late Triassic (a) and Late Triassic-Early Jurassic (b) are modified after Zhang & Tang (2009). Bold black arrows in each cross sections represent the directions of sediment transportation. The mechanisms of subsidence are labelled in red.